The Pennsylvania State University

The Graduate School

Nuclear Engineering

**NEUTRON DEPTH PROFILING MEASUREMENTS and GEANT4 SIMULATION**

**COMPARISON FOR INTEL-SEA2 BOROPHOSPHOSILICATE GLASS (BPSG)**

**SAMPLE**

A Thesis in

Nuclear Engineering

by

Dundar Ucar

Submitted in Partial Fulfillment

of the Requirements

for the Degree of

Master of Science

May 2009

The thesis of Dundar Ucar was reviewed and approved* by the following:

Kenan Ünlü
Professor of Mechanical and Nuclear Engineering Department
Director of Radiation Science and Engineering Center
Thesis Advisor

Robert M. Edwards
Professor of Mechanical and Nuclear Engineering Department

Jack S. Brenizer
J. "Lee" Everett Professor of Mechanical and Nuclear Engineering Department
Nuclear Engineering Program Chair

*Signatures are on file in the Graduate School

**ABSTRACT**

Neutron depth profiling (NDP) is a widely used near-surface analysis technique to determine the concentration versus depth profile of several technologically important light elements in almost all solid materials. The most commonly analyzed light elements are boron, lithium, and nitrogen; but several other elements can also be analyzed. NDP method is based on the energy measurements of the charged particles escaping from the surface of the sample material. Energy measurements are mostly performed by using semiconductor detectors. By using the stopping power of the sample material, depth profile of the analyzed element can be obtained by making a linear transformation of the measured energy spectrum. A few micrometer of the material can be analyzed nondestructively, and on the order of 10 nm depth resolution can be obtained depending on the material type with NDP method.

In this study, Intel-SEA2 borophosphosilicate glass (BPSG) sample was experimentally analyzed at Pennsylvania State University Neutron Depth Profiling (PSU-NDP) Facility and National Institute of Standard Technology Cold Neutron Depth Profiling (NIST-Cold NDP) Facility to calculate the $^{10}$B depth profile inside of the material. NDP measurements were obtained by using only silicon PIN Photodiode detector at PSU-NDP facility, and by using both silicon PIN Photodiode and surface barrier detector at NIST-Cold NDP facility.

PSU-NDP Facility is a part of Radiation Science and Engineering Center (RSEC) of Penn State University. In this facility, NDP experiments suffered from some specific problems. These were mainly signal noise due most likely to ground loop formation on the experimental setup and gamma content of the neutron beam. As a consequence of these problems, the measured energy spectrum of reaction products obtained from BPSG sample at PSU-NDP facility were not satisfactory enough to analyze the $^{10}$B depth profile. Therefore, NDP experiments were repeated at NIST-Cold NDP Facility. In this facility, the gamma content of the neutron beam is much less

than the one at PSU-NDP facility, and also there is no signal noise problem on the experimental setup. Therefore, better results were obtained from the NDP measurements of the BPSG sample. The thickness of the BPSG layer inside of the sample was calculated as 858 nm with surface barrier detector and 866 nm with silicon PIN Photodiode detector. Energy and concentration calibrations were made by using NIST standard reference samples.

To verify the experimental results, NDP measurements performed at PSU-NDP facility with Intel SEA2 BPSG sample were simulated by using Geant4 code. Simulation was performed at LION-XO PC cluster of Penn State University (PSU) at 15 different computer nodes. In the simulation model, it was assumed that the thickness of the BPSG layer in the silicon wafer was the measured value, which is 858 nm, by using Tennelec surface barrier detector at NIST-Cold NDP Facility. Geant4 code was very successful to predict the 1472 and 1776 keV alpha peaks in the measured energy spectrum. The net area difference between the measured and predicted alpha peaks was less than 1%. It was also successful for 1013 keV lithium peak, but not for 840 keV lithium peak. Net area difference for that peak between the measured and predicted spectra was calculated as 36%. The problem might be the cross section data set used by the code to simulate the lithium ion transport in the silicon material. Since depth profiling calculation was made by using the 1472 keV alpha peak and it was well predicted by the Geant4 code, predicted depth profile perfectly fits to the measured one. The thickness of the BPSG layer inside of the sample was calculated as 856 nm, which is very close to the measured result of 858 nm.

**TABLE OF CONTENTS**

# LIST OF FIGURES

## LIST OF TABLES

# ACKNOWLEDGEMENTS

**Chapter 1**

# INTRODUCTION

Neutron Depth Profiling (NDP) is a non-destructive, near-surface neutron analysis technique that is used to obtain the concentration distribution of a number of certain light elements along the depth in near-surface region of almost any solid material. In NDP method, a thermal or cold neutron beam is used to obtain the depth profile of the isotope from neutron induced reactions, such as (n, p), (n, α). Reaction probability is characterized by capture cross section of the sample material, and depends on the incoming neutron energy within the beam. Each particle is emitted with a constant energy which is determined by the mass balance of the reaction. The emitted particle is considered to be mono-energetic since the incoming neutron energy is very small compared to the energy of the emitted particles.

The idea of using thermal neutron beam as a spectrometer was first proposed by the Ziegler [1] in 1972. He determined range and depth parameters of boron in semiconductor silicon. Neutron depth profiling method was improved to its present capabilities by the Biersack and coworkers [2] at the Institut Laue-Langevin facility in Grenoble. Then, Downing et al. [3] compared the certain features of the NDP method with some other analytical techniques, which are secondary ion mass spectroscopy (SIMS), Fourier transform infrared spectrometry (FTIR), Auger electron spectroscopy (AES), Rutherford backscattering (RBS), Spreading Resistance Profile (SRP), etc.

NDP method has been successfully applied in many nuclear research reactor facilities in the United States [4] and all around the world today. The application of NDP method is limited by the number of available intense neutron sources, which are mainly produced in nuclear research reactors. Radiation Science and Engineering Center (RSEC) at Pennsylvania State University have a 1-MW research reactor and a Neutron Depth Profiling facility (PSU-NDP).

NDP method has been applied in this facility and previously at the University of Texas for a few technologically important samples, such as Intel-SEA2 borophosphosilicate glass (BPSG) sample and an implanted Advanced Micro Devices (AMD) silicon wafer [5, 6]. National Institute of Standard Technology (NIST) has a very well designed and successful cold neutron depth profiling facility to analyze different samples. In this study, experimental NDP measurements were performed in these facilities for BPSG sample by using different charged particle detectors, and similar results were obtained.

A computer simulation of a physical model was developed with the growth of the computer processing power. It is described as designing a model of an actual physical system and using a digital computer to execute the designed model, and to analyze the executed output. Today computer simulation is used in almost all areas of technology as a supporting tool of the mathematical modeling. Simulation approach of a model gives more flexibility and convenience. Modeling is particularly important when the system is very complex.

GEANT4 is an object oriented simulation toolkit which is used to simulate almost all kind of particle interactions in various materials by using Monte Carlo techniques. It is developed by European Organization for Nuclear Research (CERN) laboratories, and successfully applied in many areas of technology, such as high energy physics, nuclear experiments, medical, and accelerator and space physics [7]. In this study, Geant4 is mainly used for the validation and verification of depth profiling results obtained from BPSG sample inserted into Intel-SEA2 silicon wafer.

## 1.1. Motivation

Neutron depth profiling method has certain unique features compared to other analytical techniques [8]. Since the damage in the target material is very small, NDP method is considered

to be non-destructive. It is a direct consequence of the energy loss mechanism of the neutrons in the target material. Since the incoming neutron energy is very low, which is ~ 0.025 eV, small amount of momentum is carried by the neutron in the interaction, and the damage in the target material is considered to be negligible.

Another advantage of the NDP method is the absolute measurement of the depth distribution. The depth of the target material can be calculated from the residual energy of the emitted particle by using the characteristic stopping power of the material. Since the stopping power of materials is a known very accurately [9, 10], the measured depth distribution is absolute. Because of this property, it does not need calibration and beyond that it can be used as a certification method for calibrating other analytical techniques, such as secondary ion mass spectroscopy (SIMS) [11].

In order to analyze specific samples with NDP method, an intense thermal or cold neutron beam is always required. Research reactors are the main places to produce neutron high intensity beams. Neutron beams coming from the reactor core always contain epithermal neutrons and gamma rays. In PSU-NDP facility, neutron beam also contains prompt gamma rays as a result of neutron capture reactions in the hydrogen in pool water, and NDP measurements were seriously affected from these photons. On the other hand, the prompt gamma photons contribution to the neutron beam is not an important issue at the NIST-Cold NDP facility.

In the NDP method, neutron beam interacts with the analyzed isotope, and some certain reaction products are emitted. They are mainly charged particles, and measurements must be performed in vacuum environment to eliminate further energy loss in the air. However, it is not possible to satisfy ideal vacuum conditions inside the chamber, and additional energy loss as a result of interactions with air molecules is unavoidable. NDP measurements at PSU-NDP and NIST- Cold NDP facilities were performed in vacuum chambers evacuated by a turbo-molecular pump and a mechanical pump which are connected back-to-back to a flange on the lower section

of the vacuum chamber. The main problem in PSU-NDP facility is the signal noise problem due to grounding issues. This problem comes from the turbo-molecular pump connections. The system is connected more than one electrical line each with a different ground. This causes voltage difference between the lines, and ground loop problem. Detailed description and solution method of this problem will be given in Chapter **3.** At NIST-Cold NDP Instrument, this problem was not present.

In NDP measurements, there are additional uncertainties coming from the nature of experimental analysis. They can be briefly summarized as electronic noise on the amplifier chain, intrinsic noise on the detector, and energy straggling due to stochastic variation of energy loss inside the material. All of these uncertainties degrade the depth resolution of NDP measurements, which is called broadening.

Neutron depth profiling measurements of Intel-SEA2 BPSG sample were performed by Cetiner [12] at beam port #4 (BP4) of RSEC. Results of that study were very satisfactory, but they need to be improved since the measurements were seriously affected from the aforementioned problems. In order to do that, noise problem due to ground loop formation and gamma content of the neutron beam were minimized. Then, NDP measurements were repeated at PSU-NDP facility and NIST-Cold NDP facility by using BPSG sample.

Another motivation for this study is the development of a computer simulation code to verify, and also to validate the experimental results. Geant4 simulation toolkit was preferred for this study, since it has a wide range of application area to simulate almost all kind of particle interactions in several detector models, and also it has been validated through many Benchmark studies.

In Chapter **2**, the neutron energy spectrum at thermal research reactors, charged and uncharged particles, interaction mechanism of these particles in matter, the uncertainties associated with particle transport in matter, neutron depth profiling (NDP) method, and

concentration and depth profiling calculations are introduced. Chapter **3** introduces the PSU-NDP facility and NIST- Cold NDP facility, and gives detailed description of experimental setup used in NDP measurements. In Chapter **4**, a brief overview of Geant4 code and Geant4 simulation model of PSU-NDP facility are given. The experimental results obtained at PSU-NDP and NIST-Cold NDP facilities and Geant4 simulation results are given in Chapter **5**. In this chapter, also measured and predicted results are discussed and compared.

**Chapter 2**

**THEORY**

Neutron depth profiling (NDP) is a near surface neutron analysis technique. It has been successfully applied in many research facilities up to now [11, 13, 14]. NDP measurements are performed by using an intense thermal or cold neutron beam impinged on a target material. As the neutron beam passes through the material, neutron capture reactions occur at the reaction sites. Reaction products are isotropically in the material, and continuously lose energy by colliding with the host electrons while traveling through material. Then, they emerge from the surface with a decrease in energy, and are collected by charged particle detectors. The energy loss mechanism is very straightforward in the material. The average energy loss of particles along the track is determined by using the stopping power of the material. The depth distribution of the analyzed isotope is obtained by using the measured energy spectrum and the stopping power of the material.

In Section **2.1**, energy spectrum of neutrons in thermal reactors is introduced in terms of Maxwell-Boltzmann distribution. Section **2.2** gives a brief description of interaction mechanisms of radiation in matter. Also, some important definitions used to define the charged particle interaction mechanisms in matter and the origin of the uncertainties in the measurement system are explained in this section. In Section **2.3** the fundamentals of NDP method and depth and concentration calculation procedure are given.

**2.1.    Thermal Neutron Spectrum at Nuclear Research Reactors**

In nuclear research reactors, average energy of fission neutrons is approximately 2 MeV. These highly energetic neutrons are called "fast neutrons". Fast neutrons are thermalized by interacting with the nuclei of the surrounding material, which is mostly moderator. The main interaction mechanism of high energetic neutrons is elastic scattering. These neutrons have to make too many collisions with the moderator material to become thermal, because the average energy loss of neutron at each interaction is very small. Natural water is the most commonly used moderator material in the nuclear reactors, and a 2 MeV neutron makes ∼ 19 collisions in the water to slow down to 0.025 eV energy level.  After making many collisions, the energy of the neutron becomes comparable to the energy of the nuclei. Since the moderator temperature is finite and moderator nuclei is in thermal motion, thermal equilibrium is reached between collisions. This process is called *thermalization*, and the neutron in the thermal region is called *thermal neutron*. The energy of the thermal neutron is below $10^{-2}$ eV. If the neutron energy is approximately $5 \times 10^{-3}$ eV, it is called *cold neutron*. The thermal neutron velocity distribution is approximately described by the Maxwell-Boltzmann probability distribution in thermal reactors. This distribution is the expected neutron spectrum emerging from a research reactor system.

The Maxwell-Boltzmann distribution is a probability distribution function that describes the energy or velocity of an ideal gas at temperature T. This distribution gives the fractional probability that a particle will have some velocity within an interval d$v$ about $v$, and is defined as P($v$)d$v$. The velocity distribution is defined as

$$P(v) = \left[\frac{m}{2\pi kT}\right]^{3/2} 4\pi v^2 \, exp\left(-\frac{mv^2}{2kT}\right) \tag{2.1}$$

where k is the Boltzmann constant and *m* is the molecular mass of the gas. This relation is derived by using Boltzmann statistics. To find the corresponding energy distribution, we can use the transformation rule of distribution functions as follows:

$$P(v)dv = P(E)dE \, . \tag{2.2}$$

After transformation of variables from v to E, and normalization; Equation **2-1** becomes

$$P(E) = \frac{2\pi}{(\pi kT)^{3/2}} \sqrt{E} \, exp\left(-\frac{E}{kT}\right) . \tag{2.3}$$

The spectrum of fully-moderated neutrons is described by Maxwell-Boltzmann distribution. The distribution of neutrons per unit energy at room temperature ($20^{\circ}$C) is shown in Figure **2-1**. To find the most probable velocity of neutrons, we should first set the derivative of Equation **2.1** to zero and solve for velocity. Thus, the most probable velocity ($v_{max}$) of neutrons at room temperature ($20^{\circ}$C) is

$$v_{max} = \sqrt{\frac{2kT}{m}} = 2199 \, \frac{m}{s} \, . \tag{2.4}$$

Using the same procedure for Equation **2.3**, which is setting the first derivative of energy distribution function $P(E)$ to zero, and solving for E, yield the most probable energy, $E_{max}$ of neutrons at room temperature (thermal equilibrium temperature). It is calculated as

$$E_{max} = \frac{kT}{2} = 0.0254 \, eV \, . \tag{2.5}$$
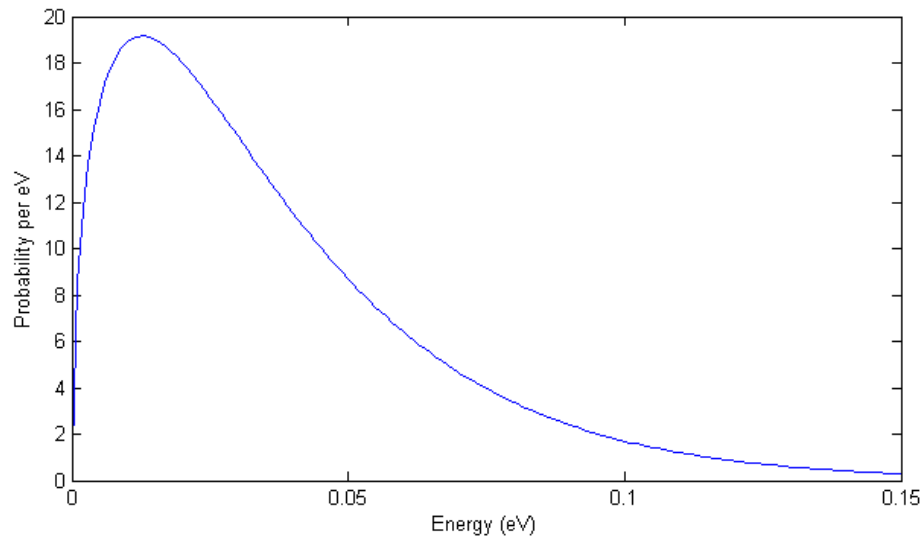


**Figure 2-1:** Maxwell-Boltzmann energy distributions of thermal neutrons at $20^{\circ}$C

**2.2.     Interaction of Radiations with Matter**

Radiation is described as the energy propagation through space or matter in forms of electromagnetic waves or energetic particles. In terms of its effect on matter, it is classified as *ionizing* and *non-ionizing* radiation. Ionizing radiation is the radiation which can remove an atomic electron or molecule in matter during interactions. It consists of x-rays, alpha particles, neutrons, beta particles, and gamma rays.  Non-ionizing radiation does not create ionization during interactions. It includes microwaves, radio waves, ultraviolet radiation, and visible light.

 Alpha, proton and beta particles are all charged particles, that directly ionize the atomic electrons through electromagnetic forces. On the other hand, neutrons are non-charged particles, and indirectly ionize the atomic electrons. In terms of the charge of the radiation, radiation is classified as *charged* and *non-charged* radiation. For non-charged particles, ionization is caused by the secondary charged particles which are produced during collisions with nuclei. Other types of directly ionizing radiation are gamma and X-rays.

If the rest mass of the charged particle is large compared to the rest mass of the electron, it is called a *heavy charged particle*. Protons, alphas, and mesons are all heavy charged particles. Electrons and positrons are called *light charged particles*.

**2.2.1.     Heavy-Charged Particle Interactions**

Heavy charged particles mainly interact with matter via electromagnetic forces. Since the nuclear force is very small compared to the Coulomb force except at low energies, it is usually ignored. Electromagnetic force is a direct result of the repulsion between positive charge of the particle and negative charge of medium atoms. As the charged particle travels inside the material, it continuously loses energy by interacting with the electron cloud of the target material. At each

collision, a small fraction of its energy is transferred from the charged particle to the orbital electron of the atom. If this energy raises the electron to a higher energy shell, this event is called *excitation* of the atom. Excited atoms decay to the lower energy state, which is called de-excitation, by releasing electromagnetic radiation. If the transferred energy is enough to overcome the electron's binding energy to the atom, it is called "ionization". As a result of ionization process, electron-ion pairs are produced inside the medium. The maximum energy that is transferred at each collision from a charged particle with mass of M and energy of E to an electron with mass of $m_e$ can be calculated as

$$T_{max} = \frac{4Mm_eE}{(M + m_e)^2} \cong \frac{4m_eE}{M} \; .$$

(2.6)

It is approximately 1/500 of the particle energy per nucleon [15]. Since the transferred energy is very low, charged particles have to make many collisions inside the material before coming to a full stop.

Heavy charged particles travel in matter in almost straight lines [16]. They cause thousands of ionization and excitation events in the matter along their tracks.

*Stopping Power:*

The linear energy loss of the charged particle per unit path length is calculated by using the linear stopping power of the material. Linear stopping power defines the average energy loss of the particle per unit path length, or average linear rate of energy loss of a charged particle in the material (MeV x $cm^{-1}$). It is defined as:

$$S(E) = -\frac{dE}{dx} \; .$$

(2.7)

Energy loss along the track of a particle is represented by Bragg curve. Energy loss rate of 5.49 MeV alpha particles per unit path length in air is shown in Figure **2.2**.
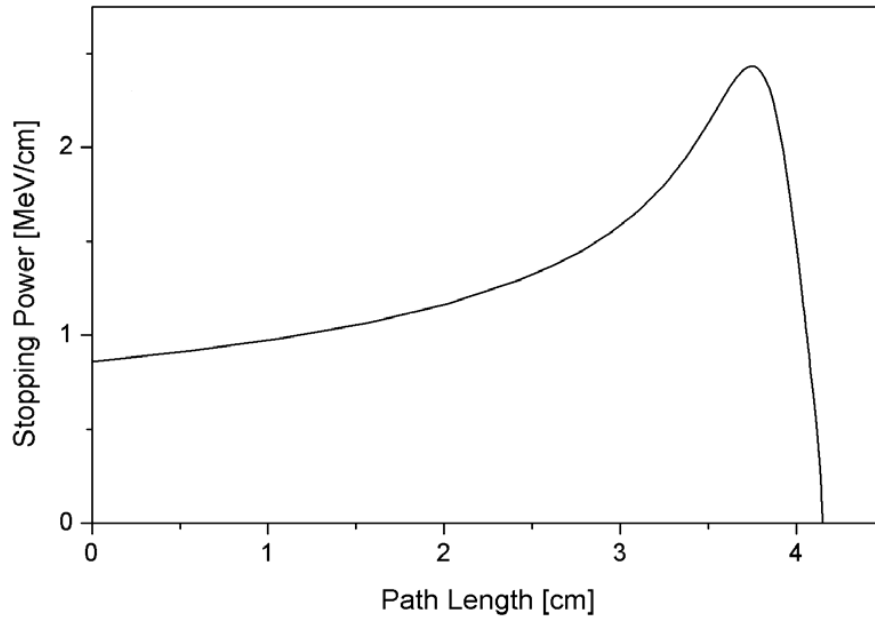
**Figure 2-2:** Energy loss rate of 5.49 MeV alpha particles in air along their paths

The classical expression which is used to define the average energy loss rate of charged particles is *"Bethe-Bloch formula"* [17]. It was developed by Hans Bethe in 1930, and is expressed as

$$-\frac{dE}{dx} = \frac{4\pi e^4 N Z_2 {Z_1}^2}{m_e v^2} \left[ \ln\left(\frac{2m_0 v^2}{\langle I \rangle}\right) - ln(1 - \beta^2) - \beta^2 + \Psi(Z_1) \right]. \qquad (2.8)$$

In this equation, E is the particle energy, $Z_1$ is particle atomic number, $Z_2$ is target atomic number, v is the particle velocity, x is the distance traveled by the particle, e is the charge of electron, $m_e$ is the rest mass of electron, N is the number density of target atoms, $\langle I \rangle$ is the average excitation and ionization potential of the target, c is speed of light and $\beta$ is relative particle velocity, *v/c*. Last term, $\Psi(Z_1)$ is Bloch's error term which is very small. The basic assumption used in the derivation of this equation is that particles interact with target atoms through Coulomb forces, and any energy loss due to nuclear reactions is negligible. It is valid for alpha and beta particles, but is

not valid for electrons. Also, it is limited to high energetic particles. At low energies, electron of target atom may be captured by the particle to neutralize its nuclear charge. To consider particle neutralization effect, many approaches were developed, and they are called *scaling laws*. Further information about this subject can be obtained from Ref. [18].

*Slowing-Down Time*

The time rate of a heavy charged particle to lose energy is calculated by using the chain rule of differentiation as

$$-\frac{dE}{dt} = \left(-\frac{dE}{dx}\right)\frac{dx}{dt} = \left(-\frac{dE}{dx}\right)v \,. \tag{2.9}$$

Slowing-down time is defined as the time it takes a heavy charged particle to stop in matter. For a particle with kinetic energy T, it can be calculated as

$$\tau \simeq \frac{T}{-dE/dt} = \frac{T}{v(-dE/dx)} \,. \tag{2.10}$$

*Range:*

Another parameter which is used to define the total path length traveled by the charged particle in matter is the range. Since particle transport in matter is a stochastic process, there are more than one definitions for range. For example, projected range $R_p$ is the particle's net penetration into the material measured along the particle's trajectory, radial range $R_r$ is the path length traveled by the particle along the radial direction, etc. Actual range is defined as the integrated distance a particle travels before coming to rest. In terms of stopping power *S(E)*, mean projected range is calculated as

$$R = \int_0^{E_i} \frac{dE}{S(E)}, \tag{2.11}$$

where $E_i$ is the incoming particle energy. This equation is valid for negligible range straggling.

For a discrete range distribution $R(x_i)$, mean projected range is approximated as

$$R = \frac{1}{N} \sum_{i=1}^{N} R(x_i), \tag{2.12}$$

where N is the number of bins.

### 2.2.2. Light Charged Particle Interactions

Light charged particles consist of electrons and positrons. There are two types of energy loss mechanism for light charged particles: collisional and radiative. Collisional energy loss is due to inelastic collision between particle and the medium atom. For this type of interactions, particles lose energy via interacting with orbital electrons. They cause many ionization and excitation events in the medium as in heavy charged particle in reactions. There is a major difference between heavy and light charged particles due to mass difference. Since light charged particles interact with a particle which has equal mass, large scattering angles are observed unlike the heavy charged particles that travel in almost straight paths.

The maximum energy transfer in a collision from an incident electron with energy E to an atomic electron is calculated as.

$$T_{max} = \frac{E}{2}. \tag{2.13}$$

Since they have equal masses, both of them are emitted with half of incident particle kinetic energy in a single collision.

Radiative energy loss of light charged particles is due to Bremsstrahlung event. It is defined as the radiation emitted due to rapid decelaration of the charged particle usually when deflected by an atomic nucleus. A photon is emitted as a result of this process. The photon energy becomes larger, as the deceleration of the particle increases. The energy of the photons often lies in the X-ray electromagnetic region. Probability of Bremsstrahlung event varies with the square of atomic number of the medium atoms and kinetic energy of the charged particles. For heavy charged particles, it is small and, thus, neglected.

***Stopping Power:***

Like heavy charged particles, the stopping power is defined as the average linear rate of energy loss of a charged particle in the material (MeV x cm$^{-1}$). There are two stopping power mechanisms for light charged particles, which are collisional and radiative. Collision stopping power is a modified version of the Bethe-Bloch formula, and is expressed as

$$\left(-\frac{dE}{dx}\right)_{col} = \frac{1}{(4\pi\epsilon_0)^2}\frac{2\pi e^4 NZ}{m_e v^2}\left\{ln\left(\frac{m_e v^2 E}{2I^2(1-\beta^2)}\right) - g(\beta^2)\right\}, \qquad (2.14)$$

where $g(\beta^2)$ is called the density effect correlation, which is function of the electron velocity. For high energetic particles, it is approximated as

$$g(\beta^2) = -(\ln 2 + 1)\beta^2. \qquad (2.15)$$

At low energies, it is defined as

$$g(\beta^2) = \ln 2 + 1. \qquad (2.16)$$

Radiative stopping power through Bremsstrahlung is approximated as

$$\left(-\frac{dE}{dx}\right)_{rad} = \frac{NEZ(Z+1)e^4}{137 m_e^2 c^4}\left\{4 \ln\left(\frac{2E}{m_e c^2}\right) - \frac{4}{3}\right\}. \qquad (2.17)$$

Total stopping power of light charged particles is the sum of collisional and radiative stopping powers,

$$\left(-\frac{dE}{dx}\right)_{tot} = \left(-\frac{dE}{dx}\right)_{col} + \left(-\frac{dE}{dx}\right)_{rad}.$$

*Range*

Since the scattering angles of the light charged particles can be very large, they do not travel in straight paths in matter. Thus the number of incident particles passing through a distance x inside the material will not be constant. There are some approaches to measure the range of light charged particles. One of them is to use continuous slowing down approximation and to neglect the energy loss fluctuations. The calculated light charged particle ranges in various materials can be found in Ref. [19].

### 2.2.3. Non-charged Particle Interactions

Neutrons, gammas and X-rays are all non-charged particles. Interaction mechanisms of non-charged particles are different than those of charged particles. A brief description of interaction mechanism of these particles in matter is explained in this section.

*Neutron Interactions:*

Neutrons mostly interact with the nucleus through nuclear forces. There are several interaction types between the neutron and a nucleus. Interaction probability is expressed using the cross section concept. Cross section, which is denoted as **σ,** is defined as the specified reaction probability between the incoming neutron and the target material in units of area (in SI units,

$cm^2$). It strongly depends on the neutron energy and the temperature of the material. The cross section of the specific interaction type decreases as the neutron energy increases at low neutron energies. The absorption cross section, in this region, is proportional to the inverse of neutron velocity for some materials, and this region is called "*1/v region*". Following 1/v region, resonance region occurs in which cross sections increase to high values which are called "resonance peaks", and then drop again. Total cross section, $\sigma_t$ defines the probability of any type of interaction between the neutron and nucleus.

The interaction type is indicated by using a simple notation. Interaction of a neutron n with a target nucleus of T, forming a resultant nucleus R and particle p is shown as T(n, p)R. For example, $^{10}B$ neutron capture reaction is denoted by $^{10}B(n, \alpha)^7Li$.

At low neutron energies, dominant reaction types are neutron induced reactions, such as capture, fission, i.e., which create secondary radiations to be detectable by any solid state detector. Since the incoming neutron energy is low, neutron induced reactions are energetically possible if the reaction Q value is positive. Neutron induced reactions, such as (n,$\alpha$), (n,p), i.e., are the basis of neutron depth profiling method.

As the neutron energy increases, probability of neutron induced reactions decreases rapidly. For high energetic neutrons, dominant interaction type is the scattering reactions. Scattering reactions can be classified as elastic and inelastic scattering. In elastic scattering, a small amount of energy is transferred from the neutron to nucleus; but total kinetic energy of the neutron and nucleus remains the same. In inelastic scattering, nucleus is excited to a higher energy level. Then, it drops to a lower energy state by releasing radiation. Thus, total kinetic energy of the reactants is less than the total kinetic energy of the products.

*Gamma Interactions:*

Gamma particles interact with matter through three processes: photoelectric effect, Compton scattering, and pair-production. In photoelectric effect, incident photon collides with an orbital electron, and transfers all of its energy to the electron. As a result, photon disappears and atom is ionized by releasing the orbital electron. Interaction probability is highest for low energy photons and high atomic number Z targets. In Compton scattering, photon interacts with an orbital electron and imparts some amount of its energy to the electron. This electron becomes free as in photoelectric effect process, but photon is scattered with a lost in its energy in this case. The scattered photon can interact with other atoms, and causes series of Compton interactions. Compton scattering probability is weakly dependent on the target atomic number, and is greater at high gamma energies than the photoelectric effect. In pair-production event, photon is transformed into an electron and a positron, and disappears. The minimum photon energy required for pair-production event is the sum of the rest mass energies of positron and electron, which is 1.02 MeV.  After the pair-production event occurs, produced electron loses its energy through ionization and Bremsstrahlung processes. The positron also causes ionization and loses it energy inside the matter. At low energies, the positron can also cause annihilation event, which is electron capture of positron and formation of two 0.511 keV photons.

### 2.2.4.   Uncertainties:

Energy loss of charged particles in matter is a stochastic process.  Even if the charged particles originate at the same depth as a result of the neutron induced reactions, they lose different amount of energy when they emerge at the same point. This is due to the fact that they make many small angle scatterings, which cause particles travel slightly different distances before

they reach to the same point. A spread of energies about the mean residual energy always occurs

[20]. The main reasons of uncertainties in NDP measurements are summarized as follows:

1. Energy and range straggling as the particles travel inside the material,

2. Detector energy broadening due to noise and stochastic nature of particle reactions
   within the detector volume, and

3. Geometric broadening due to size of the detector and the sample.

In this section, definitions and calculation procedures of these uncertainties will be

described.

*Energy Straggling:*

Energy straggling is defined as the average deviation from the mean energy loss. For low

energetic particles, energy loss and straggling is due only to valence electrons. At higher energies,

inner shell electrons also contribute to energy loss and straggling [21]. Energy straggling is

expressed as

$$\sigma_E^2 = \langle\, [\Delta E - \langle \Delta E \rangle]^2 \,\rangle\,. \tag{2.18}$$

The classical approach to model the energy straggling is Bohr formalism [22, 23] which

is expressed in SI units of Joule as

$$\sigma_{Bohr}^2 = 4\pi Z_1^2 Z_2 e^4 N x\,, \tag{2.19}$$

where $Z_1$ and $Z_2$ are atomic numbers of projectile ion and target material, respectively, N is the

atomic density of the target material, $e = 1.602\mathrm{x}10^{-19}$ C, and $x = d cos(\theta)$ is the mean path

length traveled by the particle inside the material. For compound materials, total straggling is the

sum of the straggling values coming from each compound material. This is called *additivity rule*.

The Bohr calculation is mostly used as a reference value [24].  The Bohr formula is independent

of the energy of the particle, thus energy loss straggling only depends on the mean path length.

*Range Straggling and Angular Scattering:*

The mean standard deviation from the mean projected range is defined as *range straggling*. Since

particle transport in matter is a stochastic process, range straggling always occurs. It means that

mean range of different particles projected through a material with same initial energy always

fluctuates. Range straggling is expressed by

$$\sigma_R^2 = \int_0^{E_0} \frac{d\sigma_R^2}{dl} \frac{1}{|nS(E)|^3} \, dE \, , \tag{2.20}$$

where $l$ is the path length traveled by the particle and n is the target atomic number density. For a

discrete range distribution $R(x_i)$, range straggling is approximated as

$$\sigma_R^2 = \frac{1}{N} \sum_{i=1}^{N} (R(x_i) - R)^2 \, , \tag{2.21}$$

where R is mean projected range which is given by Equation **2-12**, and N is the total number of

bins.

In case of small-angle scattering, the standard deviation of the path length due to

scattering is approximated as

$$\sigma_{ds} = d \frac{\sin(\theta)}{\cos^2(\theta)} \sigma_\phi \, , \tag{2.22}$$

where $\sigma_\phi$ is standard deviation of deflection angle, d is depth, and θ is particle emittance angle.

The energy spread due to multiple small-angle scattering is approximated as

$$\sigma_{Es} = S(E)\sigma_{ds} \, . \tag{2.23}$$

By combining Equation **2.22** and Equation **2.23**, the expression can be reduced to

$$\sigma_{Es} = dS(E) \frac{\sin(\theta)}{\cos^2(\theta)} \sigma_\phi \, . \tag{2.24}$$

The standard deviation of deflection angle can be found from [25, 26] as

$$\sigma_\phi = \frac{2Z_1 Z_2 e^2}{\bar{E} a} \frac{2}{2.35} C (\pi a^2 N l)^M .$$ (2.25)

In Equation **2.25**, **a** is called *screening radius*, and is defined as

$$a = \frac{0.855 a_0}{\left( Z_1^{\frac{2}{3}} + Z_2^{\frac{2}{3}} \right)^{1/2}} ,$$ (2.26)

where $a_0$ is 52.9Å, C and M are fitted values, and they are estimated experimentally as C= 0.3 and M=0.85 in Ref. [27]. Further information about angular scattering can be obtained from Ref. [28, 29, 30]

*Geometric Uncertainties:*

Geometric uncertainties originate from the size and orientation of the detector and the sample in the measurement system. They can be minimized unlike the uncertainties resulting in the sample material due to stochastic nature of the particle interactions. The major factor which causes geometric uncertainty is the acceptance angle $\Omega$. Detectors only accept the particles emitted into a certain solid angle, which is defined as the acceptance angle of the detector. In NDP measurement system, particles are emitted from a certain depth inside the substrate. Acceptance angle of the detector causes a spread in path length which particles travel, and energy broadening in the measured spectrum. Energy broadening due to acceptance angle can be approximated as

$$\sigma_E = S(E)\sigma_A ,$$ (2.27)

where $\sigma_A$ is the uncertainty in path length due to acceptance angle, which is expressed by

$$\sigma_A = \left[ \int_0^{\frac{\pi}{2}} d\theta \, P(\theta)(\ell - \bar{\ell}^2) \right]^{1/2} ,$$ (2.28)

where $P(\theta)$ is the probability distribution function which is normalized over all detectable

emission angles and $\bar{\ell}$ is the mean path length. The normalized probability distribution function

can be approximated as

$$P(\theta) = \frac{W(\theta)}{\int_0^{\pi/2} d\theta W(\theta)}, \qquad (2.29)$$

where $W(\theta)$ is the weighting function. The mean path length traveled by the particles and the

weighting function can be calculated as follows:

$$\bar{\ell} = \int\limits_0^{\pi/2} d\theta \, P(\theta) \, \ell(\theta) = \int\limits_0^{\pi/2} d\theta \, P(\theta) \frac{d}{\cos \theta} = d\langle cos\theta \rangle, \qquad (2.30)$$

$$W(\theta) = \int\limits_0^{R_s} dr_s \, \eta(r_s) \, \Delta\Psi(r_s, \theta), \qquad (2.31)$$

where $R_s$ is the radius of the sample, $\eta(r_s)$ is the normalized neutron intensity impinged on the

sample with radius of $r_s$, and $\Delta\Psi(r_s, \theta)$ is the detection coverage. Detection coverage can be

expressed as

$$\Delta\Psi(r_s, \theta) = 2 \cos^{-1} \frac{D^2 \tan^2 \theta + r_s^2 - R_d^2}{2r_s \, D \, tan\theta}, \qquad (2.32)$$

where D is the distance between the detector and the sample, $R_d$ is the detector radius, $r_s$ is the

emittance position, and $\theta$ is the emittance angle. This analysis was obtained from Maki et al. and

further information can be found in Ref. [31].

### *Detector Uncertainties*

Detector uncertainties are mainly due to entrance window and stochastic nature of the charge

carrier formation in the detector. In this study, semiconductor detectors, which are silicon PIN

photodiode and surface barrier detectors, were used for the NDP measurements, and thus the

detector uncertainties were analysis for these detectors. Uncertainty due to multiple small angle

scattering is very small for semiconductor detectors as compared to the other types of detectors,

and it was ignored in this analysis. The photodiode detector is a window-less detector, thus, there

is no straggling effect due to entrance window for this detector. The only uncertainty for

photodiode detector is due to the charge carrier formation. This uncertainty can be calculated

from the following equation:

$$\sigma_c = \sqrt{FE\epsilon} \, , \tag{2.33}$$

where F is the Fano factor, $\epsilon$ is the ionization potential, and E is the particle energy. For silicon

F=0.11, and $\epsilon = 3.62 \; eV$. If we consider $^{10}$B(n,α)$^7$Li interaction, the energy of the first alpha

particle is 1472 keV, and charge carrier uncertainty in PIN photodiode detector is calculated as

$$\sigma_c \approx 766 \; eV \, . \tag{2.34}$$

Theoretical model of the charge carrier collection process for silicon PIN Photodiode

detectors was analyzed by Mimura et al., and detailed information can be obtained from Ref.

[32]. In that study, straggling in electronic losses in dead layer of the silicon and fluctuations due

to energy loss caused by nuclear collisions between alpha particle and silicon were also calculated

in terms of full-width at half-maximum (FWHM) of the peak. The fluctuation caused by nuclear

collisions was predicted as 3.5 keV in FWHM for 6 MeV alpha particles, and the straggling due

to the dead layer effect was calculated as 9.9 keV in FWHM for the 2.5 μm dead layer. The

energy resolution of the detector was found as 12.6 keV in FWHM for 5.486 MeV.

On the other hand, surface barrier detectors have a very thin entrance window, which is

usually gold or aluminum coated layers. Thickness of this layer is kept very thin, typically 100

nm silicon equivalent, to minimize energy loss straggling. However, energy straggling is a little

bit higher for surface barrier detector than PIN photodiode detector due to this effect. A

comparison of the silicon PIN photodiode detector and silicon surface barrier detector is given in

Ref. [33].

### 2.2.5. Stopping and Range of Ions in Matter (SRIM)

SRIM [9] is a computer code package which is primarily used to calculate stopping and range of ions in target material by using Monte Carlo technique. The energy loss of ions in matter and final distribution of the ions after they stopped in the target material, the stopping force and range of ions in a given energy range in any target material, the mixing and cross contamination between layers, and the radiation damage from neutrons, electrons, and photons can be calculated by using SRIM code. The code contains several modules in order to do these calculations. They are Transport of Ions in Matter (TRIM), SR_Module, and Ion Stopping in Compounds and Range Statistics. TRIM is a very complex program in which eight layers of target material can be modeled. It can calculate the 3D ion distribution of ions, and also all kinetic energy loss mechanisms including damage, ionization, and sputtering in target material. The SR_Module can be used for the generation of range and stopping power at a given energy. In this study, SRIM code is used to convert the measured energy spectrum into concentration versus depth distribution of $^{10}$B atoms in borophosphosilicate glass (BPSG) sample.

There are several theories and assumptions are used in the SRIM/TRIM code to get a reasonable approximation to experimental data. Some of them are Lindhard-Scharff-Schiøtt (LSS) theory [34], Thomas-Fermi Theory (Thomas, 1927; Fermi, 1927), Wigner-Seitz model [35, 36], Brandt-Kitagawa theory [37], etc. The TRIM code estimates the range of particles inside the matter in a good accuracy by using these theories.

### 2.3. Neutron Depth Profiling (NDP) Method

In the neutron depth profiling method, thermal or cold neutrons interact with certain isotopes of some light elements and initiate exoergic nuclear reactions by neutron capture inside

the substrate material. The reaction products are mostly charged alpha or proton particles. Since neutrons are neutral particles, they can move deep into the material. This means that a few micrometers of almost any material can be analyzed by using NDP method. Table **2-1** gives the list of isotopes which undergoes neutron capture reactions and produce alpha or proton particles and recoil atoms as reaction products. The kinetic energy of the reaction products are determined by using the reaction characteristic Q value in units of MeV.

The reaction Q value can be calculated by using the mass difference between reactants and products. For a reaction in the form A(x,y)B, the Q value can be calculated as

$$Q = c^2 \left( \sum M_r - \sum M_p \right) = 931.5 \left[ \frac{\text{MeV}}{\text{amu}} \right] x \left( M_A + M_x - M_y - M_B \right), \quad (2.35)$$

where $M_r$ and $M_p$ are the rest masses in units of amu of reactants and products, respectively. This equation is the same with the excess kinetic energy of the products:

$$Q = \sum T_p - \sum T_r = T_y + T_B - T_A - T_x . \quad (2.36)$$

If the calculated Q value is positive, reaction is said to be *exoergic* or *exothermic*. In this case, nuclear mass is converted into the kinetic energy of the final products. When Q value is negative, the reaction is called *endoergic* or *endothermic*.

The kinetic energy of the charged particle is denoted as $T_C$, and the kinetic energy of the recoil atom is denoted as $T_R$. They can be determined by using the momentum and energy conservation equations in terms of reaction Q value [20] as

$$\frac{1}{2} M_C v_C^2 + \frac{1}{2} M_R v_R^2 = Q , \quad (2.37)$$

and

$$M_C v_C = M_R v_R . \quad (2.38)$$

If Equation **2.37** is substituted into Equation **2.38**, and after rearrangement for $T_C$ and $T_R$, the kinetic energy of the reaction products can be calculated as

$$T_C = \frac{M_R}{M_R + M_C} Q,$$

(2.39)

and

$$T_R = \frac{M_C}{M_R + M_C} Q,$$

(2.40)

where $M_C$ and $M_R$ are the rest masses of charge particle and recoil atom in units of amu, respectively.

In this research, Intel-SEA2 borophosphosilicate glass sample was analyzed by experimental measurement and by Geant4 simulation separately. $^{10}$B(n,α)$^{7}$Li is the interested reaction in BPSG sample. Reaction products, which are alpha particles and lithium recoil atoms, are emitted from two different energy states. These states correspond to the ground state of the $^{7}$Li with Q=2.792 MeV and to the first excited state of the $^{7}$Li with Q=2.30 MeV [20].

$$^{10}_{5}B + {}^{1}_{0}B \rightarrow \begin{cases} {}^{7}_{3}Li + {}^{4}_{2}\alpha, & Q = 2.792 \; MeV \; (\%6.3), \\ {}^{7}_{3}Li^{*} + {}^{4}_{2}\alpha, & Q = 2.310 \; MeV \; (\%93.7). \end{cases}$$

(2.41)

The kinetic energies of the reaction products listed in Table **2-1** can be calculated from Equations **2.39** and **2.40** and the mass values given in Table **2-2**.

Neutron depth profiling procedure can be summarized as follows. When a thermal or cold neutron beam passes through the target material, capture reactions occur in the regions which contain the selected target isotopes. The reaction rate is proportional to the neutron capture cross section of the nuclide. The reaction products are mostly charged particles and recoil atoms. They are emitted isotropically and monoenergetically inside the material and some fraction are emitted from the surfaces of the material. As they pass through the material, they interact with the electron clouds of the matrix, and continuously lose energy. The depth of origin of the reacted particles is directly related to the difference between the known initial energy and the measured residual energy of the particles emerging from the surface. The greater the path length charged particle travels, the lower its kinetic energy as it emerges from the surface. To eliminate further

energy loss in the air, the target chamber is kept under vacuum. The residual energy of the

particles is measured by using charged particle detectors.

**Table 2-1:** List of isotopes that undergo neutron capture reactions

| Isotope | Reaction | Energy of particles (keV) | | Cross Section (barns) | Abundance* (%) |
|---|---|---|---|---|---|
| | | Particle | Recoil Atom | | |
| $^3$He | $^3$He(n,p) $^3$H | 572 | 191 | 5333 | 0.000137(3) |
| $^6$Li | $^6$Li(n,$\alpha$) $^3$H | 2055 | 2727 | 940 | 7.59(4) |
| $^7$Be | $^7$Be(n,p) $^7$Li | 1438 | 207 | 4800 | [2.5x10$^{14}$]$^\yen$ |
| $^{10}$B | $^{10}$B(n,$\alpha$)$^7$Li | 1472  1776 | 840  1013 | 3837 | 19.9(7) |
| $^{14}$N | $^{14}$N(n,p) $^{14}$C | 584 | 42 | 1.83 | 99.632(7) |
| $^{17}$O | $^{17}$O(n,$\alpha$) $^{14}$C | 1413 | 404 | 0.24 | 0.038(1) |
| $^{22}$Na | $^{22}$Na(n,p)$^{22}$Ne | 2247 | 103 | 31000 | [4.4x10$^{15}$]$^\yen$ |
| $^{33}$S | $^{33}$S(n,$\alpha$) $^{33}$Si | 3081 | 411 | 0.19 | 0.76(2) |
| $^{35}$Cl | $^{35}$Cl(n,p) $^{35}$S | 598 | 17 | 0.49 | 75.78(4) |
| $^{40}$K | $^{40}$K(n,p) $^{40}$Ar | 2231 | 56 | 4.4 | 0.0117(2) |
| $^{59}$Ni | $^{59}$Ni(n,$\alpha$) $^{56}$Fe | 4757 | 340 | 12.3 | [1.3x10$^{20}$]$^\yen$ |

* Data obtained from Rosman et. al. [38]

¥ Values in atoms/mCi.

**Table 2-2:** Summary of the mass values used in kinetic energy calculations of α particle and Li atoms from $^{10}$B(n,α)$^7$Li reaction

| Isotope | Atomic Mass (amu) |
|---------|-------------------|
| $^1$p | 1.007825 |
| $^1$n | 1.008664 |
| $^7$Li | 7.016004 |
| $^4$He | 4.001506 |

***Depth and Concentration Calculations:***

Depth calculation of the particles emerging from the surface of the sample can be made by using the stopping power of the material. Stopping power is defined as

$$S(E) = -\frac{dE}{dx}.$$
(2.42)

Depth of the emerging particle is calculated as

$$x = \int_E^{E_0} \frac{dE}{S(E)},$$
(2.43)

and

$$d = x\cos(\theta),$$
(2.44)

where x is the shortest path length traveled by the particle, θ is the mean emittance angle, E is the energy of the emerging particle, $E_0$ is the energy of the initial particle, S(E) is the stopping power of the material, and d is the depth of origin of the emerging particle from the surface.

Path length traveled by the particle can be expressed mathematically as

$$x = \int_E^{E_0} \frac{dE}{S(E)} = \int_E^0 \frac{dE}{S(E)} + \int_0^{E_0} \frac{dE}{S(E)}.$$
(2.45)

Equation **2.45** can be simplified by using range definition as

$$x = R(E_0) - R(E).$$
(2.46)

If Equation **2.46** is substituted into Equation **2.44**, the depth of origin of the reaction is found as

$$d = [R(E_0) - R(E)]cos(\theta).$$
(2.47)

As mentioned before, the residual energies of the emerging particles are collected by charged particle detectors. Thus, an energy spectrum is obtained as a result of NDP measurement. It is then converted into a depth distribution, $d_i\{E_i\}$ using Equation **2.47**. This can be calculated as

$$d_i\{E_i\} = [R(E_0) - R(E_i)] \, cos(\theta).$$
(2.48)

A concentration calculation is performed by using a reference sample with a known implanted dose in the same geometry. For a homogenous layer with an implanted dose of D (atoms/m$^2$) and a mass density of $\rho$ (kg/m$^3$), the atomic concentration of the measured nuclide is given as

$$C = D\frac{\rho}{\mu} = \frac{D}{\delta t},$$
(2.49)

where $\mu$ is the areal density (kg/m$^2$) and $\delta t$ is the thickness of the layer.

If N number of counts is obtained from the NDP analysis, the total number of counts will be the sum of all the individual counts. It can be expressed as

$$c_T = \sum_{i=1}^{N} c_i,$$
(2.50)

where $c_i$ is the number of counts obtained from the i$^{th}$ layer.

The nuclide concentration in the i$^{th}$ layer; $C_i$, can be determined by using Equations **2.49** and **2.50** as

$$C_i = D\frac{c_i}{c_T}\frac{1}{\Delta x_i}.$$
(2.51)

If M is the total number of layers, and if it is assumed that stopping power of each layer is the same, Equation **2.51** becomes

$$C_i = M \frac{c_i}{c_T} \frac{D}{\delta t} \; .$$

<div align="right">(2.52)</div>

Concentration distribution of the measured nuclide along the depth of the material $C_i(d_i)$ can be calculated using Equations **2.48** and **2.52**. The accuracy of this process depends on the accuracy of the mass density, stopping power and range values. Sample implantation dose can be calculated by using a reference material implantation dose as

$$C_i = \frac{c_T}{(c_T)_{ref}} D_{ref} \; .$$

<div align="right">(2.53)</div>

The depth resolution can be calculated from the following formula:

$$\Delta d = \frac{\Delta E}{S_{ave}} \; ,$$

<div align="right">(2.54)</div>

where $\Delta E$ is the energy resolution at a given depth, and $S_{ave}$ is the average stopping power.

**Chapter 3**

**EXPERIMENTAL ANALYSIS of BPSG SAMPLE**

Experimental measurements of Intel-SEA2 sample by using neutron depth profiling method were performed at Radiation Science and Engineering Center (RSEC) - NDP Facility of Penn State University, and at National Institute of Standard Technology (NIST)-cold NDP Facility. In this chapter, these facilities are described along with detailed overview of experimental setups.

**3.1.     Penn State University Neutron Depth Profiling (PSU-NDP) Facility**

Radiation Science and Engineering Center (RSEC) contains many research facilities to provide research and education activities in Pennsylvania State University. The main research facility housed in RSEC is the Penn State Breazeale Nuclear Reactor (PSBR), which is the longest operating licensed reactor of USA since 1955.  PSBR is a TRIGA Mark III design and the rated power level of the reactor is 1 MWt. It contains 102 fuel rods, and these fuel rods are formed in hexagonal shape. The core of the reactor is movable and is submerged in a 7 m pool with 270,000 liters demineralized water. The reactor core can be moved against to a large tank ($D_2O$) filled with heavy water in order to obtain neutron beam from a beamport. Fission neutrons born in the core are moderated in this tank, and thermal neutrons are scattered into two of the seven existing beam ports. Thermal neutron flux was measured to be $1 \times 10^{13}$ cm$^{-2}$s$^{-1}$ at the periphery of the core and $3 \times 10^{13}$ cm$^{-2}$s$^{-1}$ at the central pin at steady-state operation at 1 MWt.

Neutron depth profiling measurements were performed on the Penn State University Neutron Depth Profiling facility (PSU-NDP) with RSEC primary beam at beam port #4 (BP4). A

schematic layout of the NDP facility is shown in Figure **3-2**. Diameter of the neutron beam is controlled by inserting collimators into the BP4, and a1.5 cm diameter was used for these measurements. The vacuum chamber was positioned in front of BP4. The neutron beam enters through one of the thin window of the chamber, and exits the chamber through the window which is opposite to the first one. The sample material was positioned between them at a 45$^o$ angle. A small fraction of the neutron beam is lost at the front window. The detector is placed perpendicular to sample surface in the vacuum chamber by using aluminum holders.

The average thermal neutron flux at target position was measured by using a single-disk chopper time-of-flight spectrometer [39], and was found as $3 \times 10^7$ cm$^{-2}$s$^{-1}$. The differential neutron flux spectrum in front of BP4 is shown in Figure **3-1**. It follows the Maxwell-Boltzmann distribution as seen in the figure.
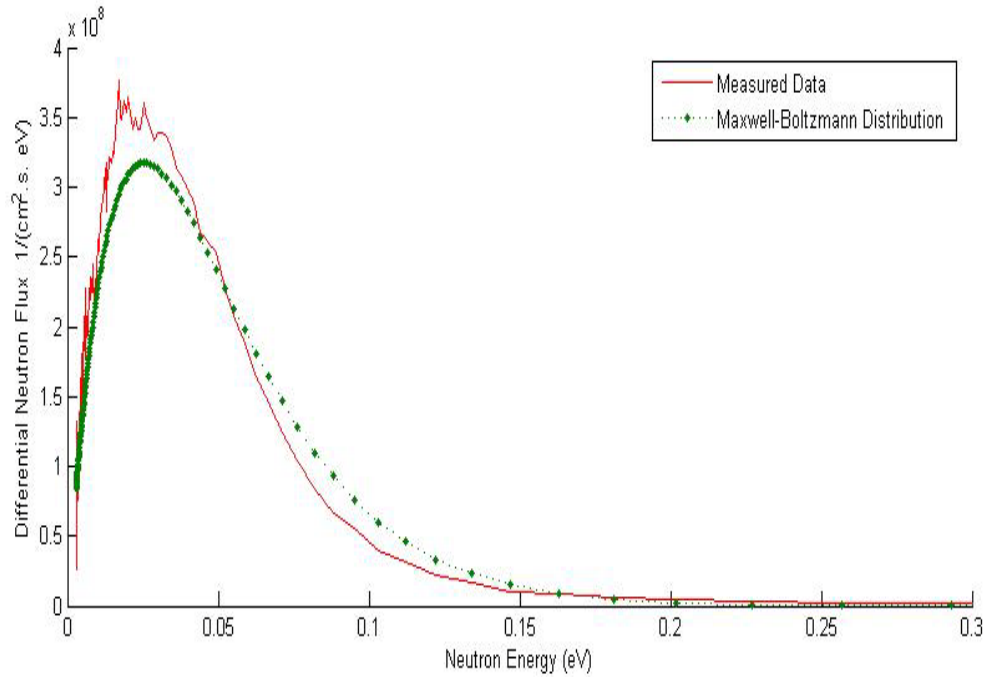


**Figure 3-1:** Differential neutron flux distribution at beam port #4 with theoretical Maxwell-Boltzmann energy distribution [39]
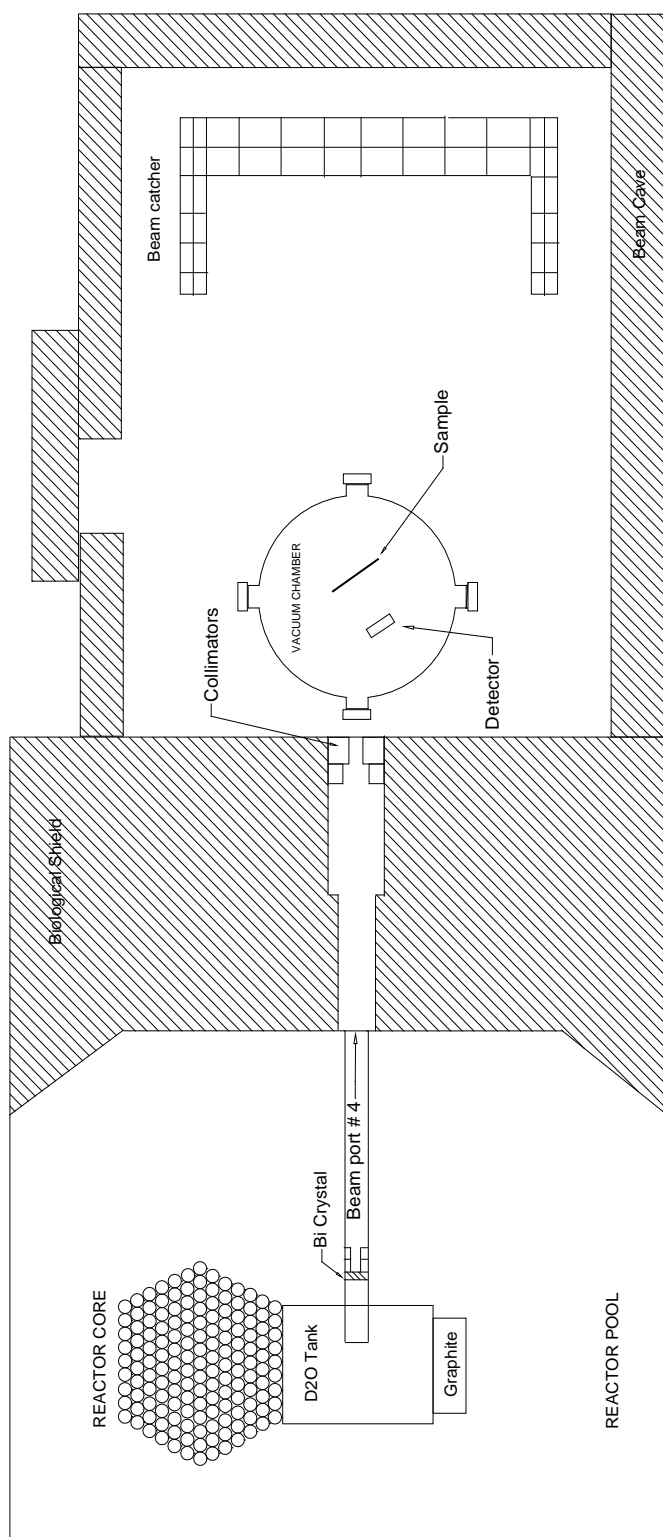
Figure 3-2: Schematic layout of the PSU-NDP Facility

**Experimental Setup**

The setup consists of a vacuum chamber, a sample material, a charged particle detector,

and the electronic equipment used for data acquisition and analysis. The vacuum chamber has

four entrance/exit ports. It is 60 cm in diameter, and is made of aluminum. The chamber's base

plate contains many feedthroughs for electrical and mechanical connections. A Leybold Turbovac

151 (C) model turbomolecular pump is placed next to a flange in the lower section of the

chamber, and is connected to a mechanical pump (roughing pump), which is a Leybold Trivac D

4B model two-stage rotary vane vacuum pump. To obtain the desired vacuum, these two pumps

are used in two stages. The mechanical pump decreases the chamber pressure down to $10^{-3}$ torr,

and then turbo-molecular pump further reduces the pressure down to $10^{-7}$ torr. A picture of the

experimental setup is shown in Figure **3-3**.



**Figure 3-3:** Picture of the NDP setup:  electronic instruments (left) and vacuum chamber (right)

NDP measurements at PSU-NDP Facility were performed for only Intel-SEA2 BPSG sample. It is a calibrated sample in which boron atoms are doped as a p-type dopant. Natural boron was used in the sample, and thus it contains $^{10}$B and $^{11}$B atoms. The abundance of $^{10}$B is known 19.9%. The BPSG sample was placed near surface of the silicon wafer.

The detectors which were used at the NDP measurements are a silicon PIN photodiode detector, a surface barrier detector, and a PIPS detector. The Hamamatsu S3590-09 silicon PIN photodiode detector was preferred due to its low signal-to-noise ratio and resolution. The silicon PIN photodiode detector is made of an intrinsic semiconductor layer sandwiched between p and n surface contacts. The usual p-layer is produced by selective area of boron, up to a thickness of 1 μm or less. Some properties of this detector, which can be found at the web page (www.hamamatsu.com) are listed in Table **3-1**. Front, top, and back view drawings are given in Figure **3-4**.

**Table 3-1:** Physical and operating properties of Hamamatsu S3590-09 silicon-PIN photodiode detector

| Parameter | | Property |
|-----------|--|----------|
| Window Material | | Windowless |
| Active Area | | 10 mm x 10 mm |
| Depletion Layer Thickness | | 0.3 mm |
| Maximum Reverse Voltage ($V_R$ Max) | | 100 V |
| Dark Current ($I_D$) : | Typical | 2 nA |
| | Maximum | 6 nA |
| Operating Temperature | | -20 to +60 $^{o}$C |

The measurement electronics consists of a Ortec-142 model charge preamplifier which is powered by a HV power supply, an Ortec model 572A amplifier, and a Ortec 550A single-channel analyzer (SCA). The preamplifier was preferred in this study because its impedance matches with the PIN-Photodiode detector's input capacitance. It is designed for low noise and fast timing for detectors with capacitance of up to 100 pF. It is optimal for alpha and beta particle spectroscopy applications.
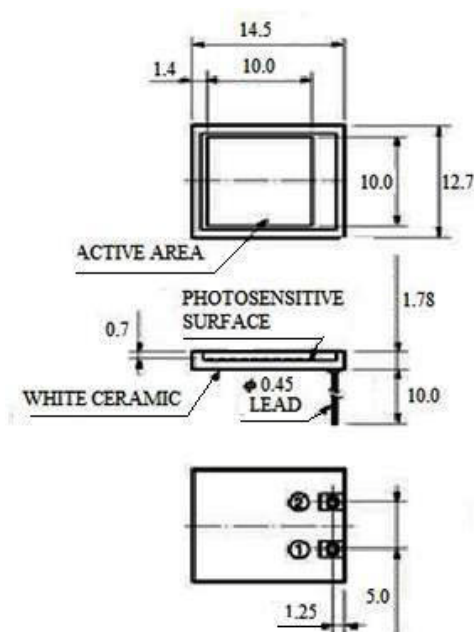


**Figure 3-4:** Drawing of Hamamatsu S3590-09 silicon PIN Photodiode detector from front, top, and back view of the detector

The Ortec 572A- model amplifier is best suited for use with silicon charged particle detectors, germanium detectors, scintillation counters, germanium detectors, and pulsed ion chambers. It includes an automatic gated baseline restorer (BLR), and a built-in-pile-up rejecter. The performance properties of Ortec 572A depend on the precision of the settings of BLR threshold.

A simplified block diagram of the measurement electronics is shown in Figure **3-5**.
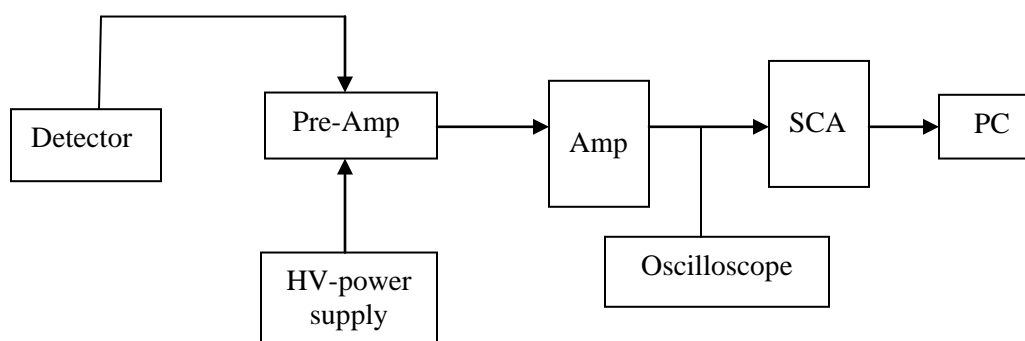


**Figure 3-5:** Block diagram representation of the measurement electronics at PSU-NDP Facility

## 3.2.    National Institute of Standard Technology (NIST) - Cold Neutron Depth Profiling Facility

The National Institute of Standard Technology (NIST) reactor is a 20 MW research reactor and it has been in operation since 1969. The NIST Cold Neutron Research facility (CNRF) was designed to develop experimental instruments for cold neutron studies in 1987, and the CNRF building was completed in 1989. The NIST Cold Neutron Depth Profiling instrument is located inside the CNRF building in beam hall. Neutron beam originates in a $D_2O$-$H_2O$ (7.5 %) ice block which is cooled by recirculating helium gas to 30-40 Kelvin. The diameter of the ice block is 36 cm, and its height is 22 cm. It has an 18 cm diameter reentrant cavity to increase the neutron flux. A lead-bismuth shield is placed to remove the gamma particles from the neutron beam, and a 13.5 cm diameter single crystal sapphire material is used to filter the slow neutron flux by 1/3 and fast neutron flux by 1/500.  Collimators are used to direct and to control the neutron beam. They are located within biological shield of the reactor and the outside of the rotating shutter shield. The shutter eliminated any background resulting from the scattered neutrons. The cold neutron flux at the sample position is measured as $1.2 x 10^9 \ cm^{-2} s^{-1}$. Schematic layout of the NIST-Cold NDP facility is given in Figure 3-6.
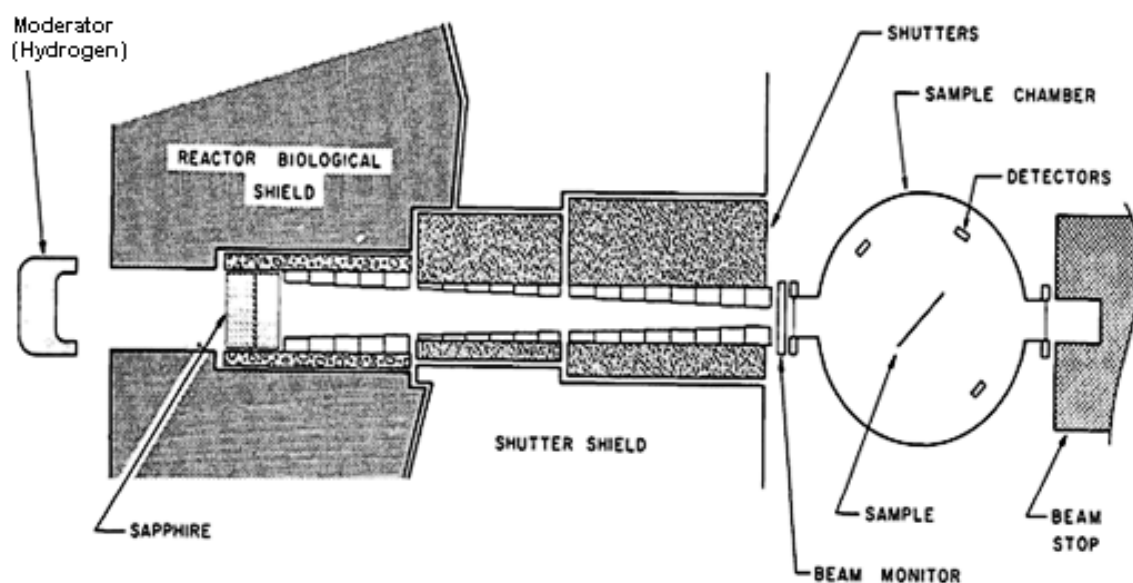
**Figure 3-6:** Schematic layout of the NIST-Cold NDP facility [13]

## Experimental Setup

The experimental cold neutron depth profiling measurements were performed in the target chamber, which is 61 cm diameter stainless steel cylinder consisting of copper gaskets at three sealing surfaces. The target chamber has many access ports for electrical and mechanical connections. The top part provides access to the sample and detector positions. The side ports, which are thin aluminum windows, are in 10 cm diameter, and neutron beam enters and exits through them. These windows can also be replaced with sapphire windows. The pressure level is reduced down to $10^{-7}$ torr level inside the chamber by using one roughing pump, one mechanical pump, and one turbo mechanical pump. The mechanical pump is back-connected through the turbo mechanical pump. The roughing pump is directly connected to the chamber. During the measurements, this pump is unplugged to eliminate the grounding problems.

The sample and detectors are mounted on motor driven base mount in which they can be positioned at any angle with 0.025 degree steps with respect to the neutron beam, independently. Multiple detectors can be mounted at every 10 degrees. They are controlled by a microcomputer. The silicon surface barrier detectors are preferred in the NDP measurements. The measured signals are transmitted to a multiprocessing minicomputer after passing through a preamplifier, an amplifier, and an analog-to-digital converter. This computer can process multiple data simultaneously.

**Chapter 4**

**GEANT4 MODEL of PSU-NDP Facility**

Geant4 is a Monte Carlo toolkit which is used to simulate almost all kinds of particle interactions in several detector geometries [40]. It has a huge application area, such as detector simulation, medical physics, space applications, etc. It is validated through many benchmark studies, and has been applied to many design and research projects all around the world. It is written in C++ language by using object oriented programming (OOP) techniques, and contains many tools to simulate almost all types of detectors and physical processes [41]. By using these tools, one can simulate the geometry of the system, the materials, the generation of primary events, the tracking of particles, the physical processes, the collection of particle inside the sensitive detectors, and the visualization of geometry and particles.

In Section **4.1**, the history of Geant4 is introduced. In Section **4.2**, a brief overview of the Geant4 design philosophy and the modules are presented. In Section **4.3**, simulation parameters are explained in detail for Geant4 model of PSU-NDP Facility.

## 4.1. History of Geant4

Geant4 project was based on improving the existing Geant3 code written in FORTRAN language by using modern computing techniques. For this purpose, a large group of scientist all around the world collaborated to construct a new code based on object-oriented programming (OOP) techniques in 1994. This project was called RD44. The main purpose of this project was to develop a detector simulation program based on modern computing tools. Then, the project's scope was enlarged to meet the requirements of the nuclear, space, accelerator, and medical

physics community. The first compact Geant4 release was completed in 1998. Up to now, several Geant4 software versions have been released under open source license. The open source license allows the user to install, use, reproduce, display, modify and redistribute the software without paying any money to the license owner. In this way, users can support the code by finding the bugs of the released version. The Geant4 version is 4.9.2, which was used in this study.

## 4.2.    Overview of Geant4

Geant4 was developed based on Booch/UML object oriented methodology. Unified modeling language (UML) is a modeling language, which is used to specify, develop, visualize, and certify the methods of object-oriented system. The Booch method is an object modeling methodology, and was developed by Grady Booch [42]. In this method, classes are created by using logical units. Geant4 uses this method with ESA Software Engineering Standards [43] in the development process by using iterative approach.

Object-oriented programming (OOP) concepts were originated in 1960s, and have continued to evolve. In an object-oriented language, applications and programs are designed by using the objects. An object is an instance of a class. It defines the data type, and also the functions of the data structure. The behavior of an object is defined by the set of methods. Classes and objects are two main concepts in OOP. OOP is defined as the interpretation of abstract data types or writing classes. Some common properties of different OOP languages can be summarized as

    i.    Polymorphism- run-time binding,

    ii.    Abstraction-providing new kinds of classes and objects from old ones, and

    iii.    Inheritance-the ability of developing new abstractions from the existing one.

Geant4 is an object oriented simulation toolkit in which users can generate a framework to design a detector setup, and then can analyze the particle interactions inside the detector. This framework consists of several modules to simulate the physical model of the system. These modules are summarized as Geometry, Physics, Run, Tracking, Detector Response, Event and Track management, Visualization and User Interface. Geant4 kernel controls all of these modules.

The geometry module gives ability to describe the detailed geometrical models, detectors, sensitive volumes, materials etc. Any geometry in the model is produced by using a number of volumes. Each volume is created by describing its shape and physical dimensions, and placing it into a containing volume. The largest one is called the world volume, and contains all the others. The shape of any volume is defined by geometrical objects, which are solids. Each volume consists of materials, which are made of elements and elements are made of isotopes. By using *G4Element* and *G4Material* classes, every material used in each volume can be described.

The physics module is used to describe all types of interactions covering wide variety of particle type and energy range. It does not provide realistic physics model, but uses mixture of models to cover all the physical interactions by using appropriate cross sections. These interactions are defined by using physical processes, which are electromagnetic, hadronic, transportation, decay, optical, photolepton-hadron, and parameterization processes. All physics processes are derived from the *G4VProcess* base class. There are three modeling approach in physics module. They are theory-driven, parameterized, and empirical formulae. In Geant4, neutron transport at energies below 20 MeV is based on empirical elastic and inelastic neutron cross section data drawn from many of the standard database sources (ENDF/B-VI, JEF, JENDL-3.2, CENDL, ENSDF, Brond, IRDF-90, MENDL, SAID, FENDL-2.2). Electronic stopping powers for α-particles and protons are based on Ziegler 1977, Ziegler 1985, and ICRU-49.

The run and event modules are used for the generation of events, to provide interfaces to event generators, and to analyze any secondary particles produced. They provide particles to be tracked to the Tracking module. The tracking is mainly used to calculate the path of particle, step size, etc. The visualization module manages the visualization of geometry, trajectories, and hits. Interface manages the production of graphical user interface (GUI), and the interactions with external software.

Detailed information about the Geant4 software can be obtained from Ref. [7].

## 4.3.    Simulation Models

The PSU-NDP Facility was modeled by using the real dimensions of the physical system and materials. Instead of modeling everything, physical system was reduced to vacuum chamber, photodiode detector, and sample only. To eliminate the neutron loss at entrance window surface, primary neutrons were emitted from an imaginary surface inside the chamber.

The vacuum chamber was defined as the world volume which contains detector, substrate and sample materials. Real chamber is very big aluminum chamber in 60 cm diameter. Since it was unnecessary to make it as big in Geant4 model, it was modeled as a small aluminum rectangular box with dimensions of [6 cm x 6 cm x 6 cm] in Cartesian geometry system. It was filled with ideal air at $2.25 \times 10^{-20}$ torr pressure and room temperature to provide vacuum environment. The substrate material is made of silicon, and contains the BPSG sample close to the surface. It was modeled with real dimensions of [2 cm x 2 cm x 1 mm], and was placed at the center of vacuum chamber with a $45^{o}$ angle to the z-axis. The BPSG sample was previously analyzed by Ünlü et al. at the University of Texas [6]. The results of that study can be summarized as follows. BPSG sample consists of 4.2 w/o natural boron and 95.8 w/o silicon materials. The boron material is homogeneously distributed inside the sample with an

implantation dose of 6.2 µg/cm$^2$. Natural boron contains %19.9 $^{10}$B and %80.1 $^{11}$B. It was modeled based on these results. The center of BPSG was placed at 460 nm depth from the substrate surface in z-direction.

Since the NDP measurements were performed by using a Hamamatsu silicon PIN Photodiode detector at PSU-NDP Facility, it is the only detector which was modeled in Geant4. The geometry and dimensions of photodiode detector are given in Figure **3-4** in Section **3.1.1**. In simulation model, it was modeled as a rectangle, which was made of silicon material, with dimensions of [10 mm x 10 mm x 0.7 mm]. It was defined as the *sensitive volume* in Geant4 to calculate the energy deposition of particles, which are alpha particles, recoil atoms, and gamma particles, entering inside of it. No voltage was applied to the detector in the simulation.

The vacuum chamber, substrate material, BPSG sample, and silicon PIN Photodiode detector were coded in "DetectorConstruction.cc". A screenshot of the Geant4 model geometry is shown in Figure **4-1**. The substrate material is in yellow color, and the BPSG sample is in red color in the figure. The green line is a neutron which is emitted from an imaginary surface inside the chamber through the target material.

The pimary particles in this model are neutrons which are in thermal energy region and, have Maxwell-Boltzmann energy distribution. The differential neutron flux distribution at BP4 of Breazeale reactor with theoretical Maxwell-Boltzmann energy distribution was given in Figure **3-2** in Chapter **3**. As seen from that figure, there are some small deviations from the Maxwell-Boltzmann distribution. In Geant4 simulation, Maxwell-Boltzmann distribution was the preferred model, because it was very hard to sample random variables governed by the real distribution. In order to do that, "*rejection*" technique (Von Neumann) was preferred due to its simplicity and effectiveness. It is a Monte-Carlo technique which is used for sampling of random variables if the analytical form of the inverse distribution, F(x) is unknown or too complex to obtain. In this

technique, probability density function (pdf), which is defined as p(x), is enclosed entirely by a

frame $P_{max}$(a-b).
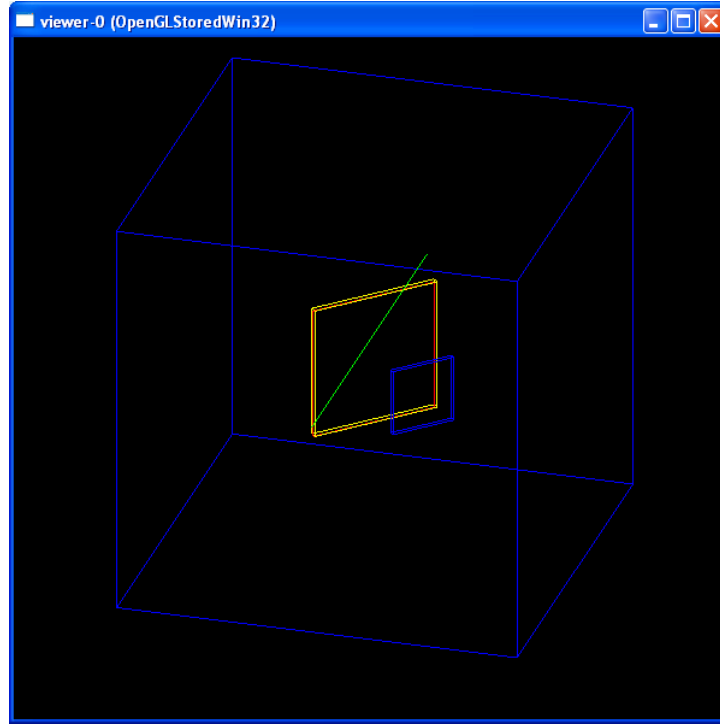


**Figure 4-1**: Screenshot illustration of Geant4 geometry model

The rejection technique can be summarized as follows. First, two random numbers, $\eta_1$

and $\eta_2$ were generated. Then, a random variable was sampled by using these two random

numbers as

$$x = a + \eta_1(b - a).$$  4.1

This random variable was accepted if

$$\eta_2 P_{max} \leq p(x).$$  4.2

Thus, the sampling was mainly made by using the area under the pdf. By using the ratio of areas,

the efficiency of rejection technique can be calculated as

$$efficiency = \frac{\int_a^b p(x)dx}{P_{max}(b-a)} \ . \hspace{3cm} 4.3$$

This technique was coded in "PrimaryGeneratorAction.cc" to sample random variables to simulate Maxwell-Boltzmann energy distribution which is given in Equation **2.1**. In our case, $P_{max}$ is 18.7165, **a** is 0.0029 eV, and **b** is 0.25 eV. In Figure **4-2**, the energy distribution obtained by using rejection technique and theoretical Maxwell-Boltzmann distribution are given. Neutrons were sent out from an imaginary cylindrical plane source, which was placed in front of the sample. Since it is known that the diameter of the neutron beam at BP4 is 1.5 cm, the diameter of the circle was modeled as 1.0 cm in the code.

The physics processes were coded in "PhysicsList.cc". Several particles and physical processes, which are electromagnetic, hadronic, transportation, and decay physics, were defined in this source file. In electromagnetic physic, gamma, electron, positron, and alpha interactions were defined by using Geant4 low energy electromagnetic package. In hadronic physics, neutron and alpha particle interactions were defined by using Geant4 low energy hadronic package. A low energy package was preferred because particle interactions occur at low energies, and also it provides better cross section data set. Some of the important classes coded in Geant4 simulation are given in Appendix **C**.

The tracking of alpha particles, gamma particles, and lithium atoms were performed in PIN Photodiode detector model. It was coded in "TrackerSD.cc". In this module, energy of each particle deposited in the detector geometry was modeled. This data, then, was stored in an output file named as "out.txt". Since millions of particles were simulated, an energy distribution was obtained as a result of this simulation. As mentioned in Section **2.3**, this distribution was converted into a depth distribution by using Equations **2.48** and **2.51**.
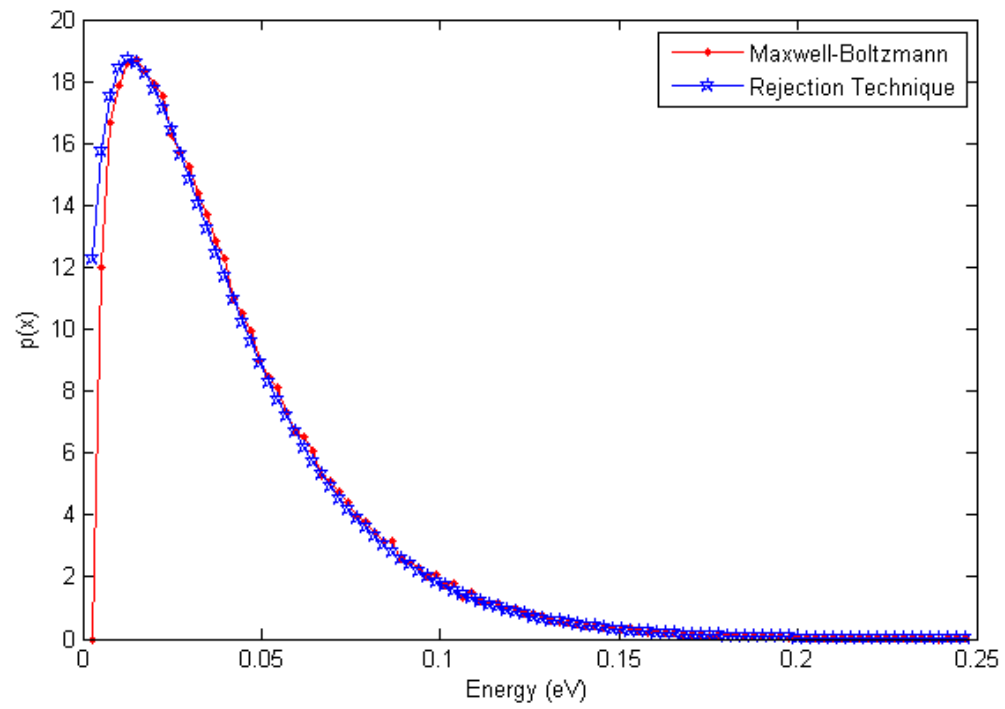
**Figure 4-2**: Simulation of Maxwell-Boltzmann probability distribution of thermal neutrons at BP4
by using Rejection technique

**Chapter 5**

**NDP EXPERIMENTAL and SIMULATION RESULTS**

In this chapter, the experimental results, that were obtained from the NDP measurements at PSU-NDP and NIST-Cold NDP Facilities, and the Geant4 simulation results for Intel-SEA2 BPSG sample are presented and discussed.

### 5.1. NDP Measurements of BPSG Sample at PSU-NDP Facility

Neutron depth profiling measurements were performed for Intel-SEA2 BPSG calibrated sample at beam port # 4 (BP4) in Breazeale Nuclear Reactor (PSBR). The measurements were made by using Hamamatsu S3590-09 model silicon PIN Photodiode detector at +20 bias voltage. The measured energy spectrum was highly affected by the gamma content of the neutron beam. In order to reduce it, the collimator was completely covered by a lead plug, which also significantly reduced the amount of neutrons at the target position. In order to increase the counting statistics, counts were taken for a long time. In the following sections, the experimental results and problems encountered during the NDP measurements at PSU-NDP Facility are presented

### 5.1.1. Experimental Problems

The NDP measurements at PSU-NDP Facility were seriously affected by some problems during the experiment. As mentioned before, these were a noise problem due to ground loop formation and the prompt gamma contamination of the beam due neutron interaction with water

behind $D_2O$ tank. In this section, effects of these problems on the measured spectrum and the possible solutions to them are discussed.

### *Ground Loop Problem*

In an electrical circuit, ground is a common reference point to measure the voltage level at another point in the loop. Ground loop occurs in an electrical system when several devices are connected to different grounds from different paths. It results in a difference in ground potential between the loops. This potential difference causes noise and interference effects on the measured energy spectrum.

At the PSU-NDP facility, this problem comes from the pump connections. Turbo-mechanical pump is connected to the vacuum chamber from a different electrical line than the measurement electronics do. However, they both have the same ground. This causes a potential difference between the lines. On the other hand, the electrical signal is carried by a signal cable through the vacuum chamber, and its ground is the same as the chamber's ground. Since the turbo pump is directly connected to a flange on the lower section of the chamber, chamber has the same ground with the pump's line, and also with the signal cable. This causes a potential difference between the signal cable and the data acquisition system. This is the main cause of the noise and interference effects on the measured signal. In Figure **5-1**, ground loop problem is illustrated. In order to eliminate this problem, vacuum chamber was isolated from the measurement electronics by using a floating shielded, double ended NW16 electrical feedthrough in which data cable transmits the electrical signal from inside of the chamber to the outside. It is directly mounted on the chamber, and provides a double shield and dielectric layer to isolate the electrical signal from the chamber. A picture of this flange is shown in Figure **5-2**. By using it, the ground loop problem
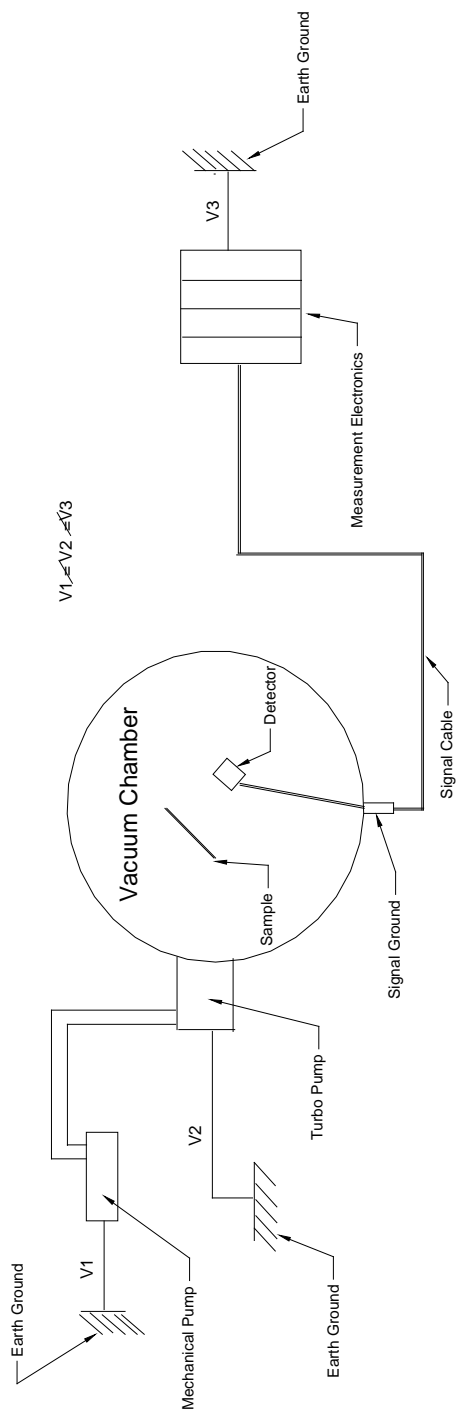
was mostly eliminated.

Figure 5-1: Ground loop problem due to electrical connections on NDP system

**Figure 5-2:** A sample drawing of the Floating Shield, Double Ended NW16 Coaxial Electrical Feedthrough

### *Hydrogen Prompt Gamma Issue*

At the Penn State Breazeale Research Reactor (PSBR), there are only two active beam ports, which are beam port # 4 (BP4) and beam port #7. The current PSBR beam port arrangement is shown in Figure **5-3**. BP4 is primarily used for neutron imaging. It was determined that BP4 has a very high gamma component due to hydrogen prompt gammas originating from neutron interactions with water behind the $D_2O$ tank, and it is impossible to get accurate results with the existing configuration. The neutron and gamma spectrum at BP4 were previously analyzed in Ref. [44]. The purpose of that study was to design a new beam port for radioscopy purposes by using MCNP code. But, it was shown that as the number of neutrons increases in the port, gamma flux also increases in the beam.

In order to eliminate gamma content of the neutron beam, there are new active studies to design a new beam port filter and collimators in PSBR. Main source of the gamma flux in the neutron beam is the capture of the thermal neutrons by the hydrogen in pool water. As a result of these reactions, highly energetic (~2.2 MeV) prompt gamma particles are emitted isotropically inside the pool. If they are emitted in the direction of BP4, they contribute to the neutron beam.

One of the future design considerations is to put a shielding material behind the $D_2O$ tank. Another design consideration is to put a sapphire crystal filter into the BP4 in order to eliminate high energetic neutrons and gammas. These projects are still under development.
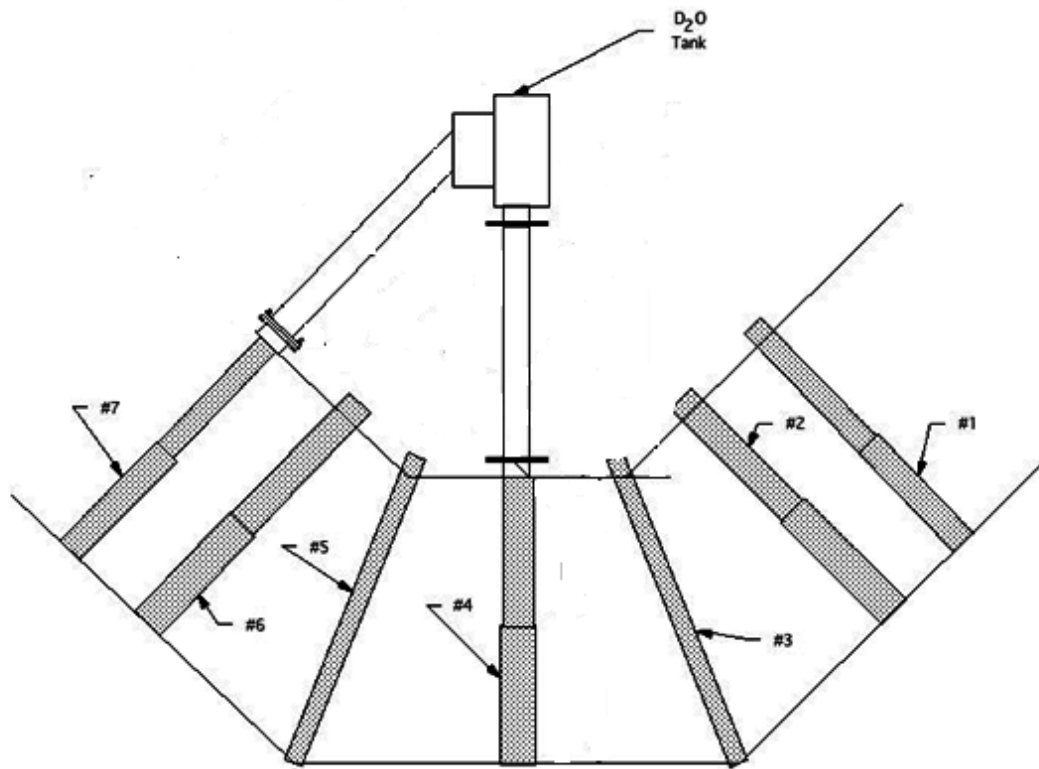


**Figure 5-3**: Current PSBR Beam Port Arrangement

### 5.1.2.  Experimental Results at PSU-NDP Facility

In this section, NDP measurement results obtained at PSU-NDP Facility are given. The measured energy spectrum is given in Figure **5-4**. The 1472 keV and 1776 keV alpha peaks are located very close to each other, and 840 keV and the 1013 keV lithium peaks cannot be observed

in the spectra, as seen from this figure. The main reason of this situation is the aforementioned problem, which is the gamma content of the neutron beam. This result is not sufficient enough to accurately calculate the concentration distribution of the $^{10}$B atoms along the depth of BPSG sample. Therefore, an energy and concentration calibration was not performed to obtain the depth profile of $^{10}$B atoms in BPSG sample. It was decided to repeat the experiment at NIST- Cold NDP facility, which is superior as compared to PSU-NDP facility.
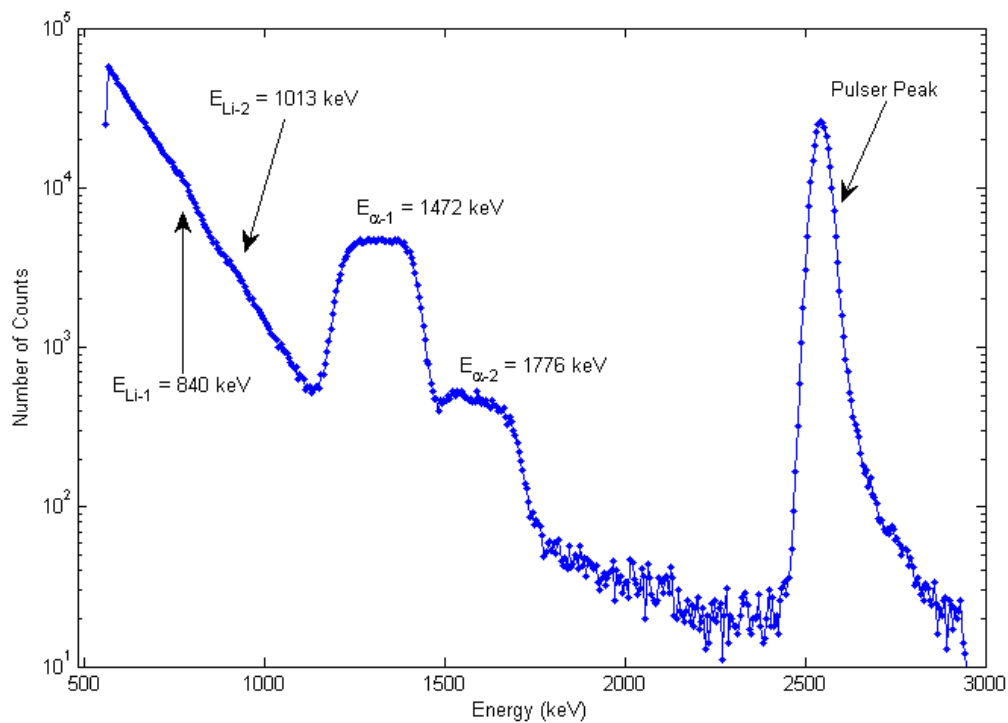


**Figure 5-4:** Energy spectrum of Intel-SEA2 BPSG sample obtained by using PIN Photodiode detector at PSU-NDP Facility

**5.2.    NDP Measurements of BPSG Sample at NIST- Cold Neutron Depth Profiling Facility**

In this facility, NDP experiments were first performed by using the Intel-SEA2 BPSG sample and surface barrier detectors, which are always used at NIST- Cold NDP Facility. The

detectors are Tennelec TP-150-75-30-NH-S model surface barrier detectors, and operate at +30

bias voltages. Then, measurements were repeated by using Hamamatsu S3590-09 silicon PIN

Photodiode detector at +20 bias voltages without changing the equipment settings. This detector

is the same detector used at PSU-NDP facility. Electronic equipments used in these experiments

can be summarized as follows: Tennelec TC 170 model preamplifier, Tennelec TC 244 model

amplifier, and Tennelec TC 953 model high voltage power supply. As mentioned before, beam

ports at NIST- Cold NDP facility are not affected by the prompt gamma particles, thus gamma

contribution to the measured spectrum was smaller in this facility.

**5.2.1.  NDP Measurements of BPSG Sample by Tennelec Surface Barrier Detector**

The depth profiling measurements of BPSG sample were first performed by using

Tennelec surface barrier detectors. The pressure level inside the chamber was $2 \times 10^{-6}$ torr, and a

40-minute count was taken during the experiment. In Figure **5-5**, total number of counts versus

channel spectrum obtained from this measurement is shown for 4096 channels. Then, channel

axis was converted to the energy axis by making energy calibration. The energy calibration was

made by using a NIST standard reference material (NIST SRM-93A), and calibration procedure

is given in Appendix **A.** The total number of counts versus energy spectrum is given in Figure **5-6**. The ratio of the alpha peaks at 1472 keV and 1776 keV energies is $\frac{94}{6} \cong 15.70$. By calculating

the total area under the two measured alpha peaks, this ratio was calculated as 14.70.

To calculate the $^{10}$B implantation dose in the BPSG sample, another standard reference

material (NIST SRM-N6) was used. Dose and concentration calculation procedures are given in

Appendix **B**. $^{10}$B concentration distribution in BPSG sample was obtained by using 1472 keV

alpha peak in measured energy spectra, and it is shown in Figure **5-7**. The thickness of the BPSG

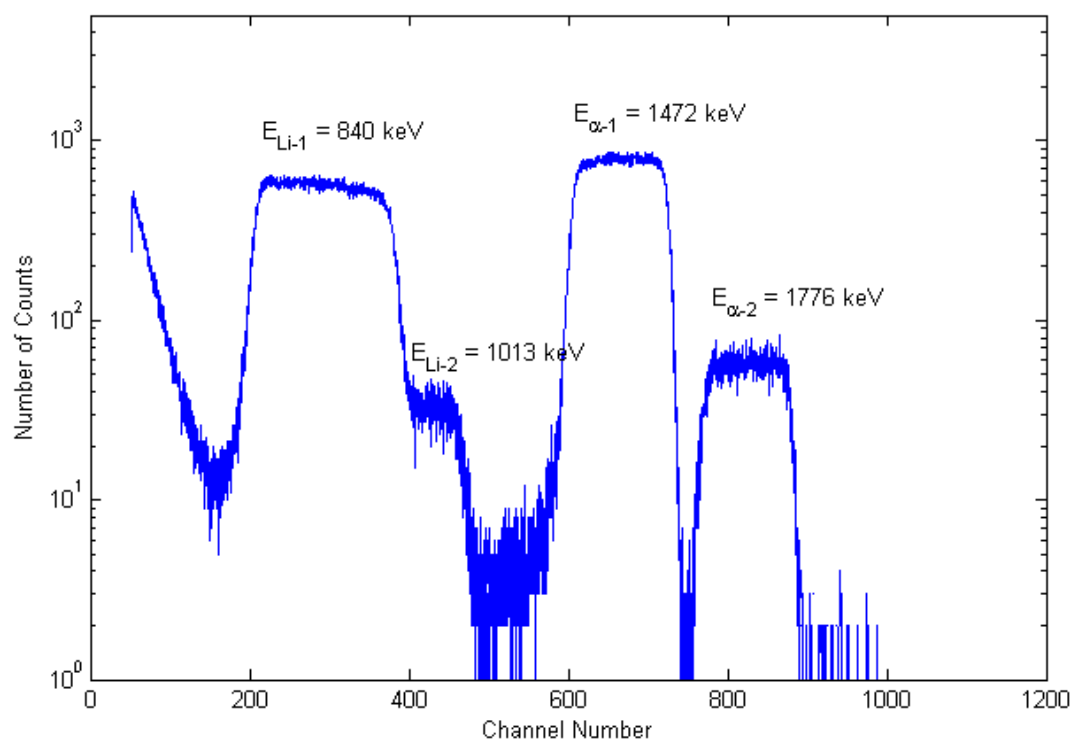sample was calculated as ~ 858 nm by using the FWHM of the distribution as shown in the figure.



**Figure 5-5:** Count versus channel spectrum of Intel-SEA2 BPSG sample obtained by using Tennelec Surface Barrier detector at NIST-Cold NDP Facility
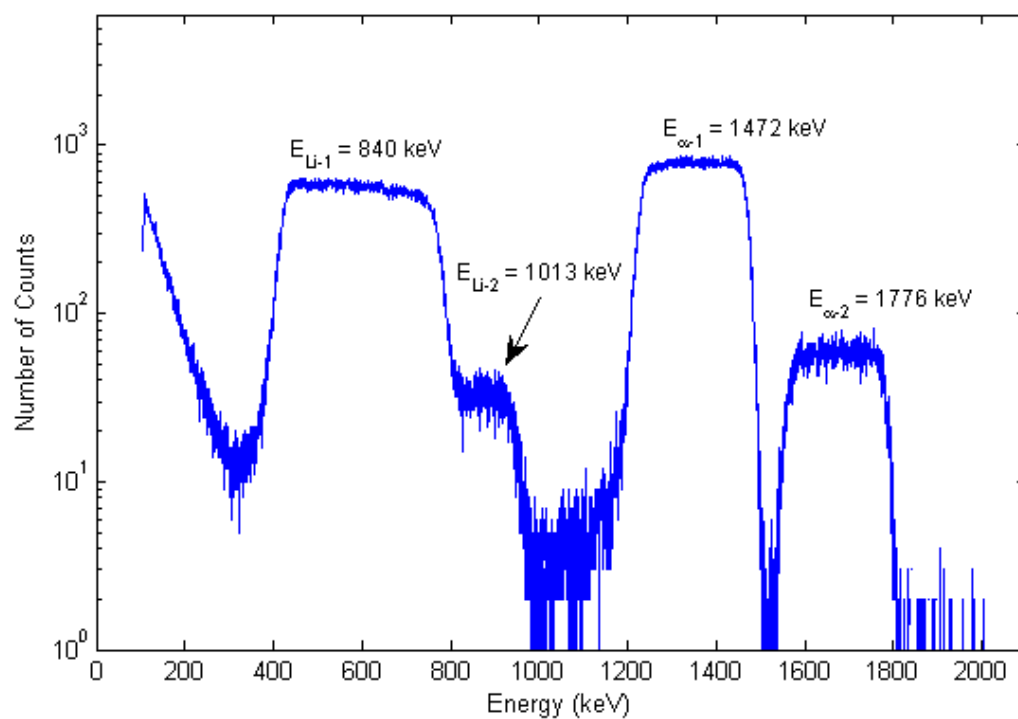
**Figure 5-6**: Energy spectrum of Intel-SEA2 BPSG sample obtained by using Tennelec surface barrier detector at NIST-Cold NDP Facility

**Figure 5-7:** Boron concentration profile of BPSG sample obtained by using Tennelec surface barrier detector at NIST-Cold NDP Facility

### 5.2.2. NDP Measurements of BPSG Sample by using Hamamatsu silicon PIN Photodiode Detector

The NDP measurement of BPSG sample was then repeated by using Hamamatsu silicon PIN Photodiode detector. Experiment was performed at $2x10^{-6}$ torr pressure level inside the chamber, and a 2.33-hour count was taken during the experiment. The total number of counts versus channel spectrum is given in Figure **5-8** for 4096 channel. In order to calculate the energy spectrum and the depth profile, the exactly same procedure given in the previous section was applied. The total number of counts versus energy spectrum is shown in Figure **5-9**, and $^{10}$B depth profile is shown in Figure **5-10**. By calculating the total counts under two measured alpha peaks, the ratio of alpha peaks was calculated as 14.72 in this case, which is almost the same with the

previous result. The thickness of the sample was calculated as ~ 866 nm by using the FWHM of the profile.
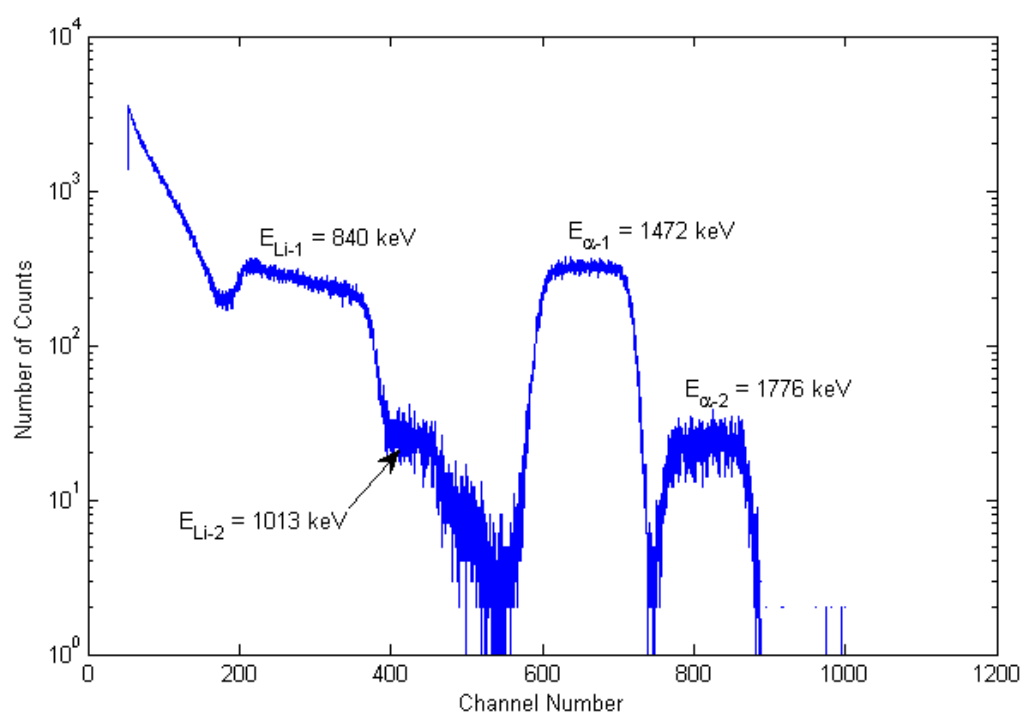


**Figure 5-8:** Count versus channel spectrum of Intel-SEA2 BPSG sample obtained by using silicon PIN Photodiode detector at NIST-Cold NDP Facility
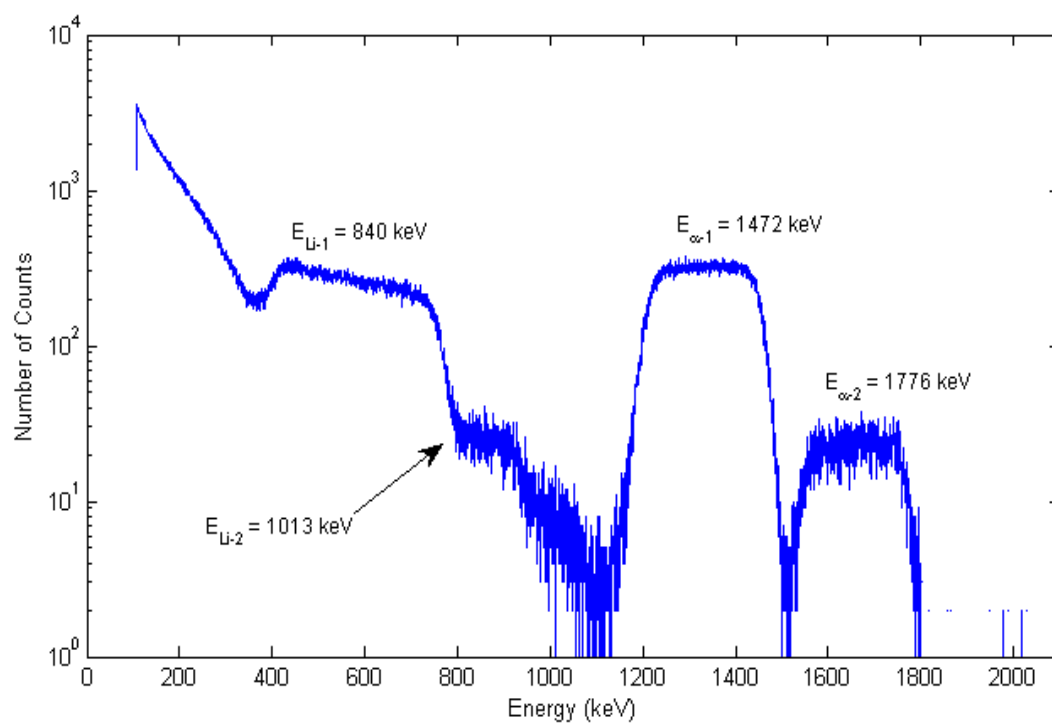
**Figure 5-9**: Energy spectrum of Intel-SEA2 BPSG sample obtained by using silicon PIN Photodiode detector at NIST-Cold NDP Facility
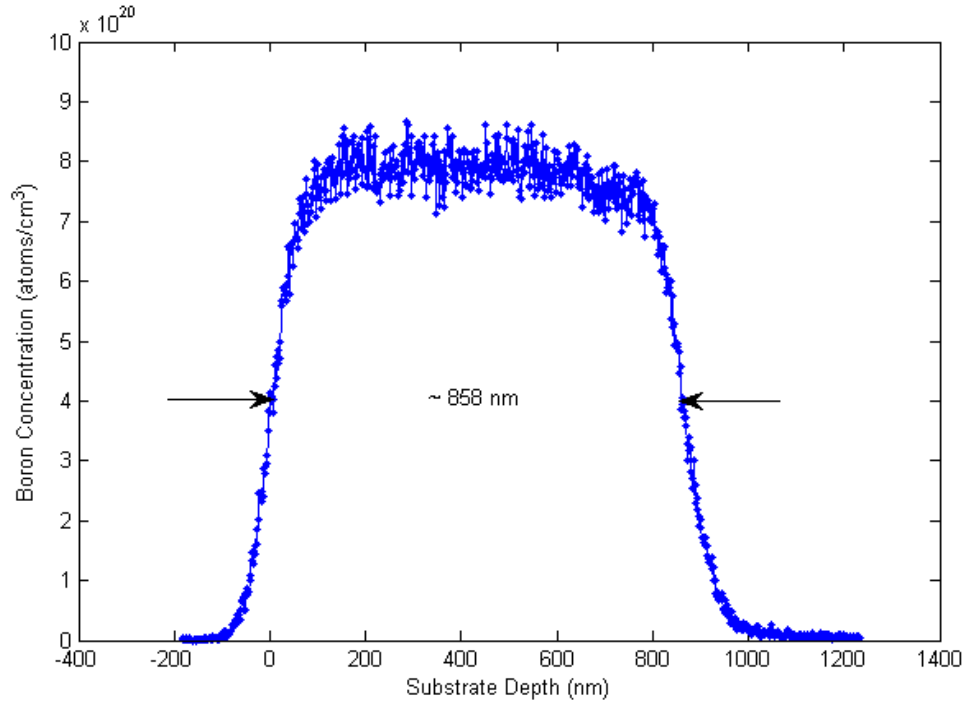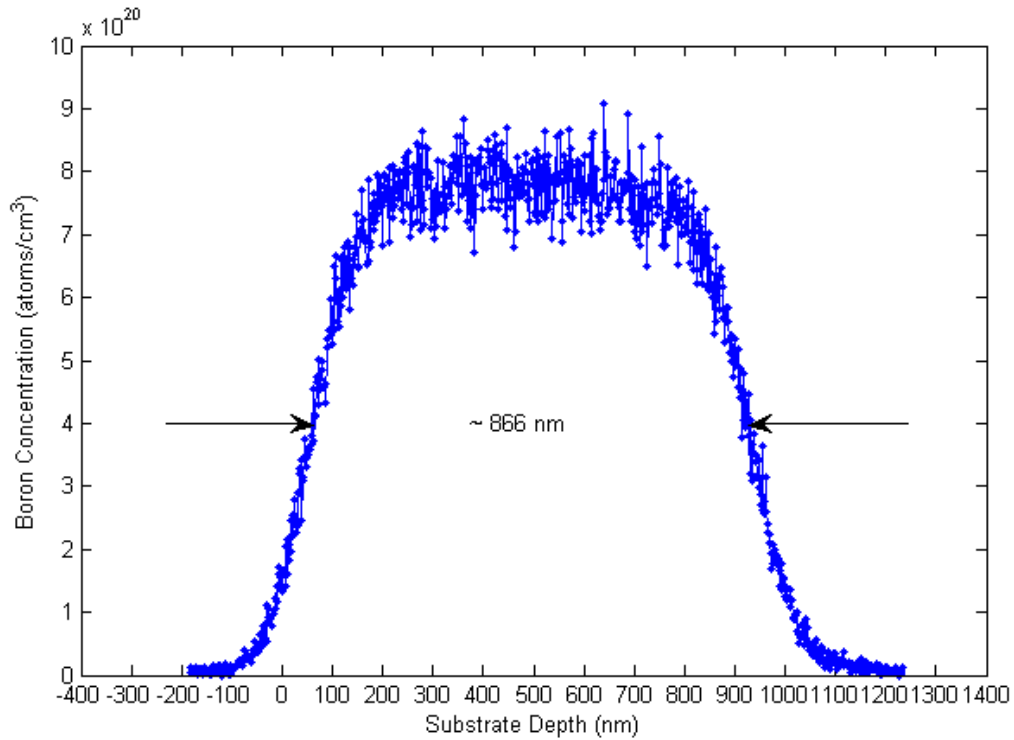
**Figure 5-10**: Boron concentration profile of BPSG sample obtained by using silicon PIN Photodiode detector at NIST-Cold NDP Facility

### 5.2.3. Calculation of Uncertainties in Experimental NDP Measurements

The theory of uncertainties in the measurement system is given in Section **2.2.4**. As mentioned in there, they are categorized as sample, geometry, and detector uncertainties. In this section some of these uncertainties are given.

To calculate the uncertainties resulting in the BPSG sample, only the 1472-keV alpha particles were considered. Energy loss straggling in the sample was calculated by using the Bohr formalism given in Equation **2.19**. It was assumed that alpha particles were emitted at a depth of

400 nm inside the sample, and the atomic density of silicon is the same as the density of bulk silicon, which is $4.996 \times 10^{22}$ cm$^{-3}$. Then, it was calculated as 3.75 keV for the minimum direction cosine ($\theta = 0^o$). The energy straggling due to multiple small-angle scatterings inside the sample was calculated by using Equation **2.23**. It was found as 0.028 keV. As mentioned before, geometric uncertainty is only a result of acceptance angle of the detector. To calculate energy broadening due to acceptance angle, Equation **2.27** and also the depth information obtained by Tennelec surface barrier detector was used. Its value was calculated as ~ 0.054 keV. Uncertainties resulting in PIN photodiode detector are given in Section **2.2.4**.

The energy resolution of silicon PIN Photodiode detector is given as 15 keV for 2 MeV alpha particles in Ref. [45]. The stopping power of silicon was calculated as 234 keV/micron by using the TRIM code. The depth resolution was calculated as 64 nm by using Equation **2.54**.

## 5.3.    Geant4 Simulation Results

In this section, simulation results are given for the Geant4 model of the PSU-NDP Facility, which is defined in Section **5.3**.  A Geant4 simulation was performed in LION-XO PC cluster of Penn State's Academic Services and Emerging Technologies (ASET) by using 15 different computer nodes. In the Geant4 model, $1.29 \times 10^{10}$ mono-directional neutrons were sent out from the source to the sample. Some of these neutrons were captured by the $^{10}$B atoms in the BPSG sample, and caused neutron capture reactions. Reaction products, which are alpha particles, lithium recoil atoms, and low energy gamma particles, were emitted in random directions, and $\sim 9 \times 10^5$ reaction products were counted by the photodiode detector. Kinetic energy of each particle/or recoil atom entering into the detector model was collected, and then stored in a text file named *"out.txt"*.

In order to convert calculated energy values into an energy spectrum, it needs to be known that how the measured energy of each particle/or atom is distributed in a real spectra obtained in multi channel analyzer (MCA). In measured spectrum, energy axis is given in 4096 channel. By using the energy calibration data, energy bin of each channel was calculated as 0.5079 keV from the measured energy spectrum. Then, the total number of counts at $i^{th}$ channel was calculated by using the following algorithm.

$$count(i) += 1 \;\; if \; \begin{cases} E(k) < i * 0.5079 \\ E(k) > (i-1) * 0.5079 \end{cases} \;\; for \;\; k = 1, 2, ...., N \; , \qquad 5.2$$

where N is the number of stored kinetic energy values in the output file. This calculation was performed by writing a Matlab script. It is given in Appendix **D**. Then, energy spectrum of the emitted particles was obtained as shown in Figure **5-11**.

The $^{10}$B concentration distribution along the depth of substrate material was calculated by using the same procedure with the experimental analysis. It is given in Figure **5-12**. The thickness of the sample was calculated as ~ 856 nm. By using the total area under the two measured alpha peaks, which are at 1472 keV and 1776 keV, the ratio was calculated as 15.45, which is closer to the known value of 15.7 than the experimental results. The predicted sample thickness differs by 0.2% from the measured value.
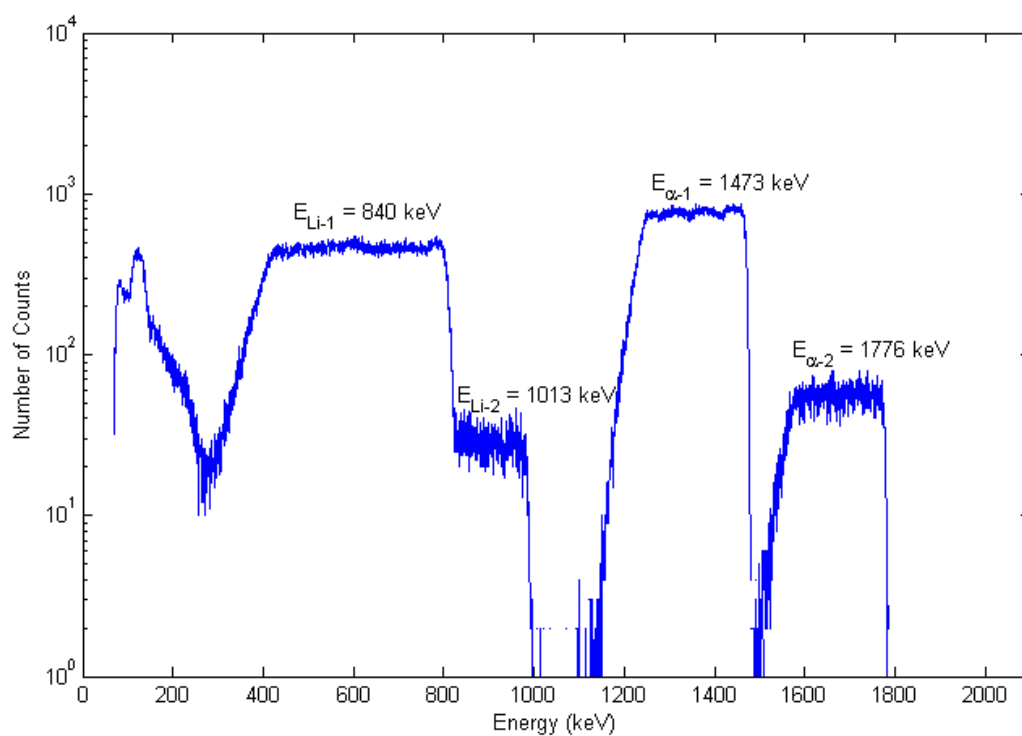
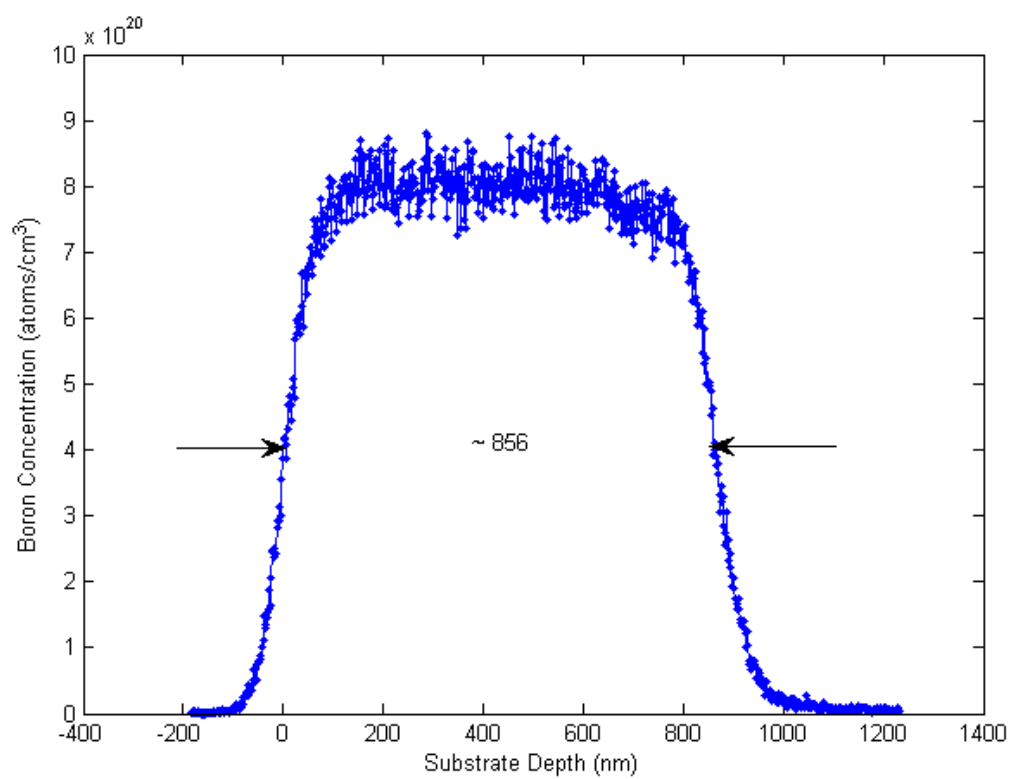**Figure 5-11**: Energy spectrum of Intel-SEA2 BPSG sample obtained by using Geant4 simulation toolkit

**Figure 5-12**: Boron concentration profile of BPSG sample obtained by using Geant4 simulation toolkit

## 5.4. Comparison of Results

The lithium peaks on measured energy spectrum results from PIN photodiode and surface barrier detectors at NIST-Cold NDP Facility have some differences especially at low energy region. This is mainly due to backscattered gamma particles. The depletion depth of the photodiode detector is 300 microns. It is approximately 9 times higher than the depletion depth of the Tennelec surface barrier detector, which is 35 micron. This causes the backscattered gamma particles to be better collected by the photodiode detector. Thus, gamma contribution to the measured spectrum is higher for photodiode detector at low energy region.

Geant4 simulation of PSU-NDP Facility was performed by using Tennelec surface barrier detector result, since backscattered gamma particle contribution to the energy spectrum is lower for this detector. Because of this, Geant4 results are compared with the results from this detector. A comparison of measured and predicted energy spectrum is shown in Figure **5-13**. As seen from the figure, Geant4 code is very successful to predict the 1472 keV and 1776 keV alpha, and 1013 keV lithium peaks. However, measured and predicted 840 keV Li peaks have some differences from each other. As mentioned in Chapter **4**, Geant4 chooses the best cross section dataset from many databases to simulate the physical interaction of the particle/or atom inside the matter. Possible explanation for this situation can be the selection of poor cross section data set by Geant4 code to simulate low energetic Li atom transport in silicon material. It was reported to the code developers, and it may be fixed in a future version. Furthermore, backscattered gamma continuum at low energy region is very well estimated by Geant4. The net area difference under the 1473 and 1776 keV alpha peaks are less than %1 between the experimental and predicted spectrums; but, it becomes %36 for 840 keV lithium peak, and %6 for 1013 keV lithium peak.

Like experimental analysis, depth profiling calculation was performed by using the 1472 keV alpha peak in the predicted spectrum for Geant4 simulation. Since similar results were

obtained for alpha peaks as shown in Figure **5-13**, predicted concentration profile of $^{10}$B in BPSG

sample by the Geant4 code is almost same with the experimental one. Comparison of depth

profiling results is given in Figure **5-14**. The net area under the peaks differs by 1% from each
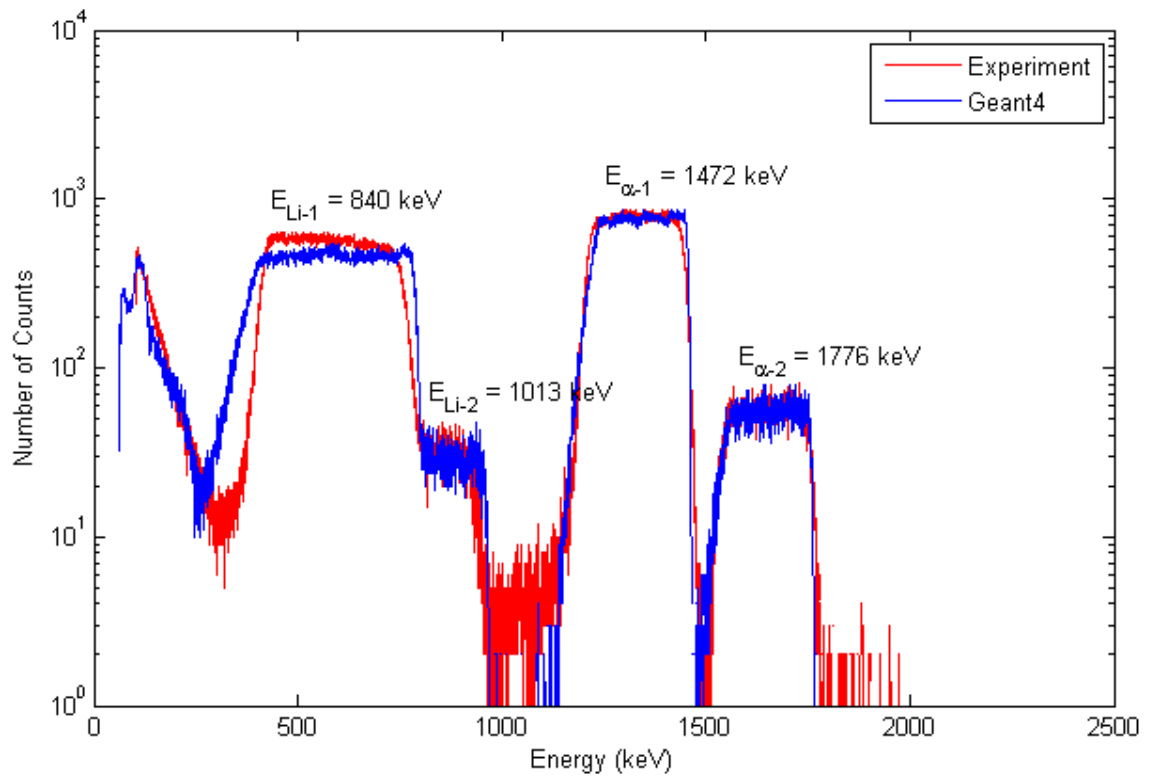
other.



**Figure 5-13**: Geant4 simulation and experimental (Tennelec surface barrier detector) energy
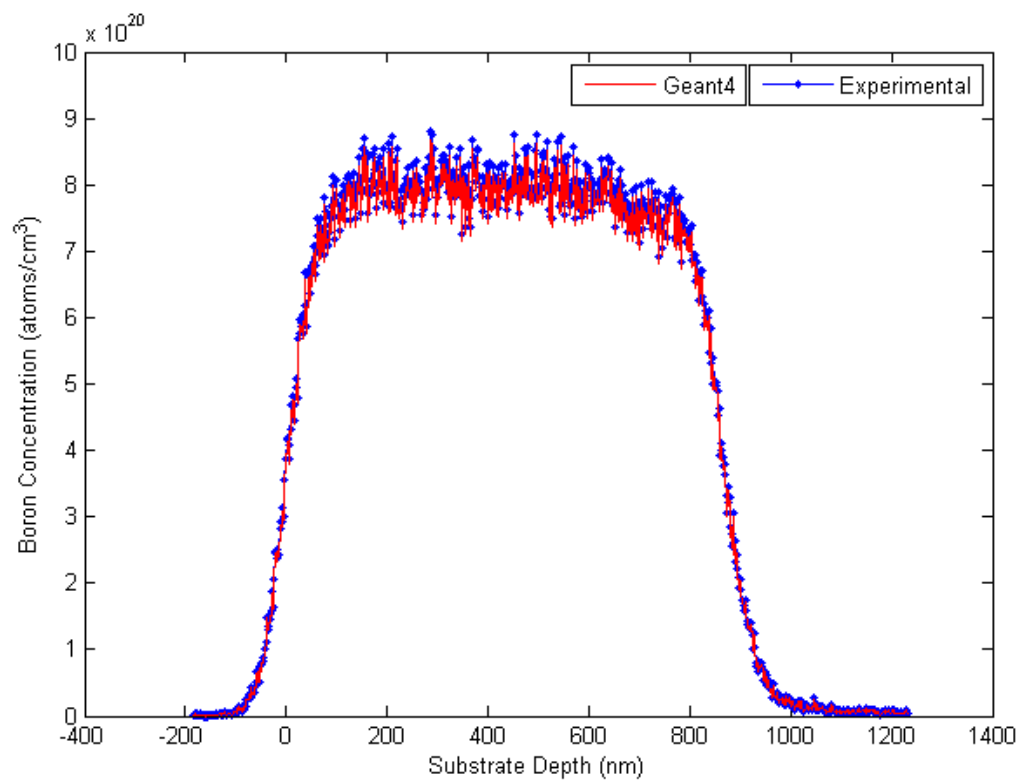spectrum results

**Figure 5-14:** Geant4 simulation and experimental (Tennelec surface barrier detector) depth profiling results

**Chapter 6**

**Summary and Conclusion**

Neutron depth profiling (NDP) method is a very successful technique to determine the concentration distribution of several light elements in any substrate material. In Table **2-1**, some of the important light elements analyzed by NDP method are listed. In this study, concentration distribution of $^{10}$B element in the borophosphosilicate glass (BPSG) sample is nondestructively analyzed by NDP method. BPSG sample is inside of silicon material at near surface region. Experimental measurements were performed at Penn State University Neutron Depth Profiling (PSU-NDP) facility and National Institute of Standard Technology Cold Neutron Depth Profiling (NIST-Cold NDP) facility. To verify the experimental results, Geant4 code was used to model the PSU-NDP facility, and to simulate the NDP measurements of BPSG sample in this facility.

NDP measurements at PSU-NDP facility suffered from some specific problems that avert to satisfactorily analyzing the BPSG samples. As mentioned before, these are mainly electrical noise problems and gamma contribution to the measured energy spectrum. Electrical noise problem was due to ground loop formation on the experimental setup, and was eminated by mounting a double-ended floating shield coaxial electrical feedthrough on the vacuum chamber. However, prompt gamma problem is due to ineffective shielding at beam port #4 (BP4), and therefore this problem can only be eliminated by changing the beam port configuration. There are new studies to change the design of the beam port on RSEC. It is planned to repeat the NDP analyzes of Intel-SEA2 BPSG sample in this facility again, after the gamma problem is solved.

NIST has a very well designed NDP Facility, and this facility does not have any electrical and gamma problems unlike the PSU-NDP facility. Additionally, it has several standard samples,

which are used to accurately make concentration and energy calibrations. A BPSG sample was analyzed by using two detectors in this facility: a Hamamatsu silicon PIN photodiode detector and a Tennelec surface barrier detector. Depletion depth of the photodiode detector is approximately 9 times higher than the thickness of the surface barrier detector. This causes better collection of low energetic backscattered gamma particles, and therefore loss of information on measured energy spectrum. Thus, experimental results obtained with surface barrier detector were better than the one obtained with photodiode detector. The thickness of the BPSG sample was calculated as 858 nm by using the surface barrier detector, and 866 nm by using the photodiode detector.

The Geant4 simulation was very successful at predicting the alpha peaks in the measured energy spectrum. The simulation results were compared with the experimental results from Tennelec surface barrier detector. The net area difference between the measured and predicted alpha peaks are less than 1%. It was also successful in predicting the 1013 keV lithium peak, but 840 keV lithium peak differs 36% from the measured one. The possible explanation might be bad cross section data set usage in the Geant4 code for the transport of low energetic lithium atoms inside the silicon substrate. On the other hand, backscattering gamma particles were predicted very well in the low energy region of the spectrum. Since depth profiling calculation was performed by using the 1472 keV alpha peak and it was well predicted by Geant4 simulation, $^{10}$B depth profile was calculated almost the same with the measured one. The net area difference between the predicted and measured profiles is less than 1%. Based on these results, it can be concluded that Geant4 code can be used as a simulation toolkit for neutron depth profiling analysis of samples containing $^{10}$B element to verify the experimental results.

Geant4 model of the PSU-NDP Facility can be used to simulate other sample material suited NDP method. As mentioned before, Geant4 code uses energy dependent cross section data sets to simulate the particle transport inside the matter. These data sets are basically obtained by

experimental measurements and interpolation. Accuracy of the simulation depends on the accuracy of the cross section data set used by the code. Therefore, application of Geant4 simulation to other samples is limited by this constraint. To simulate a sample containing other important light elements listed in Table **2-1** at PSU-NDP Facility, first of all sample material should be analyzed experimentally to calculate the implantation dose of the element by using a standard sample material. Then, sample material must be modeled by using this calculated value. Other parameters can be easily changed in the simulation model if needed.

The main constraint of the NDP method is the limited depth resolution of the measurements. Depth of a few micrometer of the material can be analyzed nondestructively, and on the order of 10 nm depth resolution can be obtained depending on the material type by using NDP method. Main application area of NDP method is semiconductor industry. The rapid progress in this industry requires higher precision in different applications. Therefore, new methods that can provide higher depth resolution are required for sensitive depth profiling measurements. Ion time-of-flight neutron depth profiling is an alternative spectroscopy technique which was first proposed by Schweikert [46]. At PSU-NDP Facility, development of a time-of-flight spectrometer was attempted [12]. That study was also suffered from the aforementioned problems in the facility. Therefore, experiments were performed by using an alpha source ($^{210}$Po), not neutron beam. After the gamma problem at BP4 is resolved, it will be possible to continue that work. Also, it is planned to use Geant4 code to simulate the new spectrometer design.

## REFERENCES

[1]    Ziegler, J. F., B. Crowder, G. Cole, J. Baglin, and B. Masters (1972) "Boron atom distributions in ion-implanted silicon by the n; $^4$He nuclear reaction," *Applied Physics Letters*, 21(1), pp.16-17

[2]    Biersack, J. P., D. Fink, and S. Datz (1975) "Channeling, blocking, and range measurements using thermal neutron induced reactions," *Plenum Publishing Corporation, New York; Hahn-Meitner Inst., Berlin, United States*, pp. 737-747

[3]    Downing, R. G., J. T. Maki, and R. F. Fleming (1987) "Analytical applications of neutron depth profiling," *Journal of Radioanalytical and Nuclear Chemistry*, 112(1), pp. 33-46.

[4]    Niveyard, G. H., and L. M. Falicov (1984) "National facilities for research in the physics of condensed matter," *Review of Scientific Instruments,* 55(4), pp 620-630

[5]    Ünlü, K., B. W. Wehring, T. Z. Hossain, J. K. Lowell (1997) " Concentration and Depth Measurements of Boron in Semiconductor Materials using Neutron Depth Profiling," *Diagnostics Techniques for Semiconductor Materials and Devices*, 3322, pp. 458

[6]    Ünlü, K., M. Saglam, B. W. Wehring (1999) "Helium-3 and Boron-10 Concentration and Depth Measurements in Alloys and Semiconductors using NDP*, " Nucl. Inst. and Meth. in Phys. Research A*, 422 , pp. 882

[7]    Agostinelli, S., J. Allison, K. Amako, et. al. (2003) "G4- simulation toolkit," *Nuclear Instruments and Methods in Physics Research Section A: Accelerators, Spectrometers, Detectors and Associated Equipment*, 506 (3), pp 250-303

[8]    Ehrstein, J. R., R. G. Downing, B. R. Stallard, D. S. Simons, and R. F. Fleming (1984) "Comparison of Depth Profiling $^{10}$B in Silicon using Spreading Resistance Profiling, Secondary Ion Mass Spectrometry, and Neutron Depth Profiling," *ASTM International*, pp. 409-425

[9]    Ziegler, J. F. (1977)  "The stopping and Range of Ions in Matter," *Pergamon Press Inc., New York, 2*

[10]   Ziegler, J. F. (1999) *"*Stopping of energetic light ions in elemental matter,*" Journal of Applied Physics,* 85 (3)*,* pp. 1249–1272

[11]   Downing, R. G., G. P. Lamaze, J. K. Langland and S.T. Hwang (1993) "Neutron depth profiling: Overview and description of NIST facilities," *Journal of Research at the National Institute of Standards and Technology*, 98(1), pp. 109-121

[12]   Cetiner, S. M. (2008) "Development of an ion time-of-flight spectrometer for neutron depth profiling", Ph.D. Dissertation, Pennsylvania State University

[13]   Lamaze, G. P., H. Chen-Mayer, J. K. Langland and R. G. Downing (1997) "Neutron Depth Profiling with the New Cold Neutron Source," *Surface and Interface Analysis*, 25, pp. 217-220

[14]   Ünlü, K., B. W. Wehring (1997) " Neutron Depth Profiling Applications at The University of Texas Research Reactor,*" Journal of Radioanal. Nuclear Chemistry* 217(2), pp. 273-278

[15]   Krane, K. S. and  D. Halliday (1987) "Introductory Nuclear Physics," *John Wiley and Sons, New York*, 1, pp. 383

[16]   Biemond, J., R.L. Lagendijk, and R. M. Mersereau (1990) *Proceedings of the IEEE*, **78**, pp. 856–883

[17]   Bethe, H. A., (1930) "Zur Theorie des Durchgangs schneller Korpuskularstrahlen durch Materie", *Ann. d. Physik,* **5**, pp. 325

[18]   Selberg, N., C. Biedermann, H. Cederquist (1996) "Semiempirical scaling laws for electron capture at low energies," *Physical Review A: Atomic, Molecular, and Optical Physics*, 54(5), pp. 4127-4135

[19] Fasso, A., K. Göbel, M. Höfert, J. Ranft and G. Stevenson (1996) "Comments on 'A new method to determine ratios of electron stopping powers to an improved accuracy'," *Phys. Med. Biol.,* 45, pp. 785-788

[20] Knoll, G. F. (2000) "Radiation Detection and Measurements," *John Wiley and Sons, (New York*,3, pp.30, 33, 507

[21] Arbo, D. G., M.S. Gravielle, J.E. Miraglia, J.C. Eckardt, G.H.Lantschner, M. Fama, and N.R. Arista (2002) *Physical Review A*,65, 042901

[22] Bohr, N. (1915) "Decrease of speed of electrified particles in passing through matter," *Philosophical Magazine*, 30, pp. 581

[23] Bohr, N. (1948) "The penetration of atomic particles through matter," *J. Komm. Hos. E. Munksgaard, Kopenhavn*, pp 144

[24] Neufeld, J. (1954) "Bohr's theory of energy losses of moving charged particles," *Physical Review A*, 95 (5), pp. 1128-1133

[25] Sigmund, P. and K. B. Winterbon (1974) "Small-angle multiple scattering of ions in the screened Coulomb region. I. Angular distributions," *Nuclear Instruments and Methods*, 119(3), pp. 541-557

[26] Gemmell, D. S. (1974) "Channeling and related effects in the motion of charged particles through crystals," *Rev. Mod. Physics*, 46(1), pp. 129-227

[27] Spahn, G. and K. O. Groeneveld (1975) "Angular straggling of heavy and light ions in thin solid foils," *Nuclear Instruments and Methods*, 123(3), pp. 425-429

[28] Meyer, L. (1971) "Plural and Multiple Scattering of Low-Energy Heavy Particles in Solids," *Phys. Status Solid*, 44(1), pp. 253-268

[29]   Amsel, G., G. Battistig, and A. L'Hoir (2003) "Small angle multiple scattering of fast ions, physics, stochastic theory and numerical calculations," *Nuclear Instruments and Methods in Physics Research B*, 201, pp. 325-388

[30]   Belery, P., T. Delbar, and G. Gregoire (1981) "Multiple scattering and energy straggling of heavy ions in solid targets," *Nuclear Instruments and Methods*, 179(1), pp. 1-9

[31]   Maki, J. T., R. F. Fleming, and D. H. Vincent (1986) "Deconvolution of neutron depth profiling spectra," *Nuclear Instruments and Methods in Physics Research B*, 17, pp. 147-155

[32]   Mimura, M., N. Hasebe, S. Kobayashi, M. Miyajima, T. Doke, and E. Shibamura (2008) "Ultraviolet-sensitive windowless silicon PIN photodiodes for alpha-ray spectrometry," *Jpn. J. Appl. Phys.*, 47, pp. 1740-1741

[33]   Zhang, Y.  and H. J. Whitlow (2002) "Response of Si p-i-n diode and Au/n-Si surface barrier detector to heavy ions," *Nuclear Instruments and Methods in Physics Research B*, 190, pp. 383-386

[34]   Lindhard, J., M. Scharff, and H. Schiøtt (1963) "Range concepts and heavy ion ranges. Notes on atomic collisions, II-Low velocity heavy ion ranges and relation to quasi-elastic atomic collisions between ions and atoms," *Kgl. Danske Vid. Sels. Mat.-Fys. Medd*, 33, pp. 1

[35]   Wigner, E.P. (1942) *Physics Division* (U.S. Atomic Energy Commission Report CP-387), pp. 4

[36]   Wigner, E.P. (1986)  *Journal of Applied Physics*, 17, pp. 857

[37]   Brandt, W. and M. Kitagawa (1982) "Effective stopping-power charges of swift ions in condensed matter," *Phys. Rev. B*, 25(9), pp. 5631-5637

[38]  Rosman, K. J. R. and P. D. P. Taylor (1998) "Isotopic Compositions of the Elements 1997," *Journal of Physical and Chemical Reference Data*, 27, pp. 127-1287.

[39]  Niederhaus, J. H. (2003) "A single-disk-chopper time-of-flight spectrometer for thermal neutron beams," *M.S. Thesis, Pennsylvania State University*

[40]  RD44 Collaboration (1998), CERN/LHCC, 98-44

[41]  Geant4 Collaboration (1999), http://wwwinfo.cern.ch/asd/geant4/G4UsersDocuments/UsersGuides/PhysicsReferenceManual/html/index.html

[42]  Booch, G. (1994) "Object-oriented Analysis and Design with Application," *Benjamin/Cummings Pub., Inc.,* 2

[43]  Amako, K., J. Apostolakis, G. Cosmo, S. Giani, P. Urban (2002) "GEANT4: OO Toolkit for Particle Detector Simulation", *User Requirements Document 6.4*

[44]  Alim, F., K. Bekar, K. Ivanov, K. Ünlü, J. Brenizer and Y. Azmy (2007) "Modeling and optimization of existing beam port facility of PSBR," *Annals of Nuclear Energy*, 33(17-18), pp. 1391-1395

[45]  Simon, A., G. Kalinka (2005) "Investigation of charge collection in a silicon PIN photodiode," *Nuclear Instruments and Methods in Physics Research Section B: Beam Interactions with Materials and Atoms*, 231(1-4), pp. 507-512

[46]  Schweikert, E. A. (1989) "Advances in nuclear analysis methods," *The analyst*, 114(3), pp. 269-274

**Appendix A**

**Energy Calibration**

In Figure **5-5**, total number of counts obtained from $^{10}$B(n, α)$^{7}$Li reactions at BPSG

sample is given at 4096 channels. In order to convert this count distribution into an energy

spectrum, an energy calibration was performed using the NIST standard reference material

(SRM-93A). It is a high-boron borosilicate glass wafer with dimensions of 32 mm length and 6

mm diameter. Energy calibration steps can be summarizes as follows:

[1] Two edges corresponding to two alpha peaks at 1472 keV and 1776 keV were located as
shown in Figure **A-1**, which shows the measured energy spectrum both from both BPSG
sample and SRM-93A sample.

[2] A Fourier function was fitted to one of the edges (1472 keV) as shown in Figure **A-2**.

[3] To find the center of the peak (zero-crossing point), fitted function was differentiated
once. Then, center of peak was found as channel 2900. This number corresponds to the
channel number at FWHM of the peak.

By repeating this procedure, the center of 1776 keV alpha peak was found at channel 3500, and

then the relation between the energy and channel was calculated as

$$E(keV) = 0.7636 + 0.5073 * channel$$

Then, this equation was used to calculate the energy spectrum of BPSG sample, and also

to plot the energy spectrum from Geant4 simulation results.
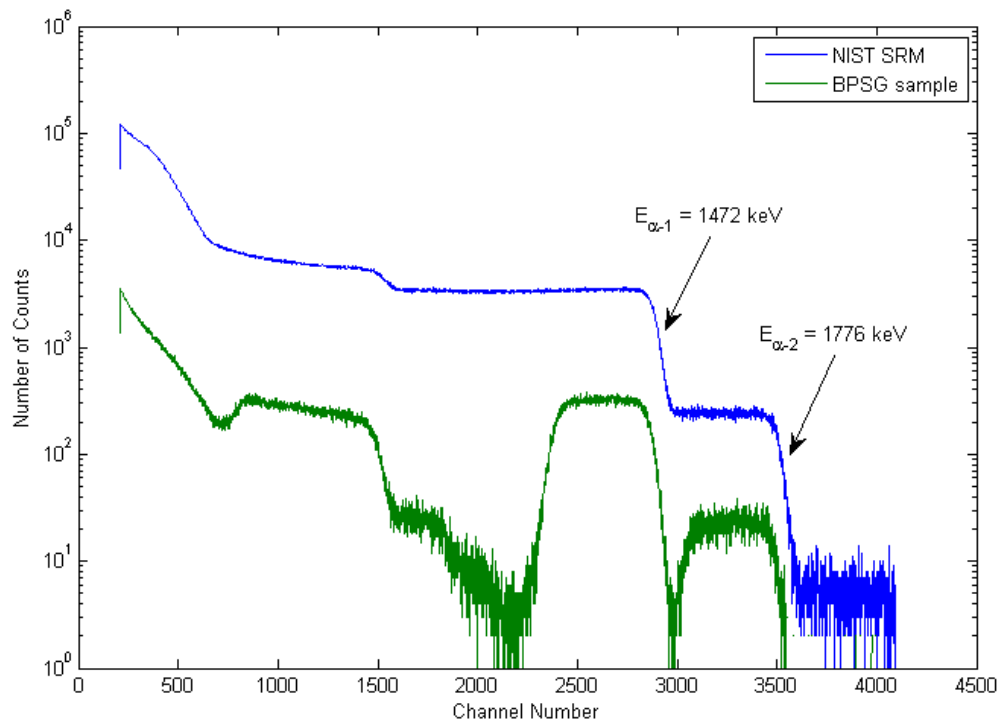
**Figure A-1**: Energy spectrum of Intel-SEA2 BPSG and SRM-93A samples obtained by using Tennelec surface barrier detector at NIST-Cold NDP Facility
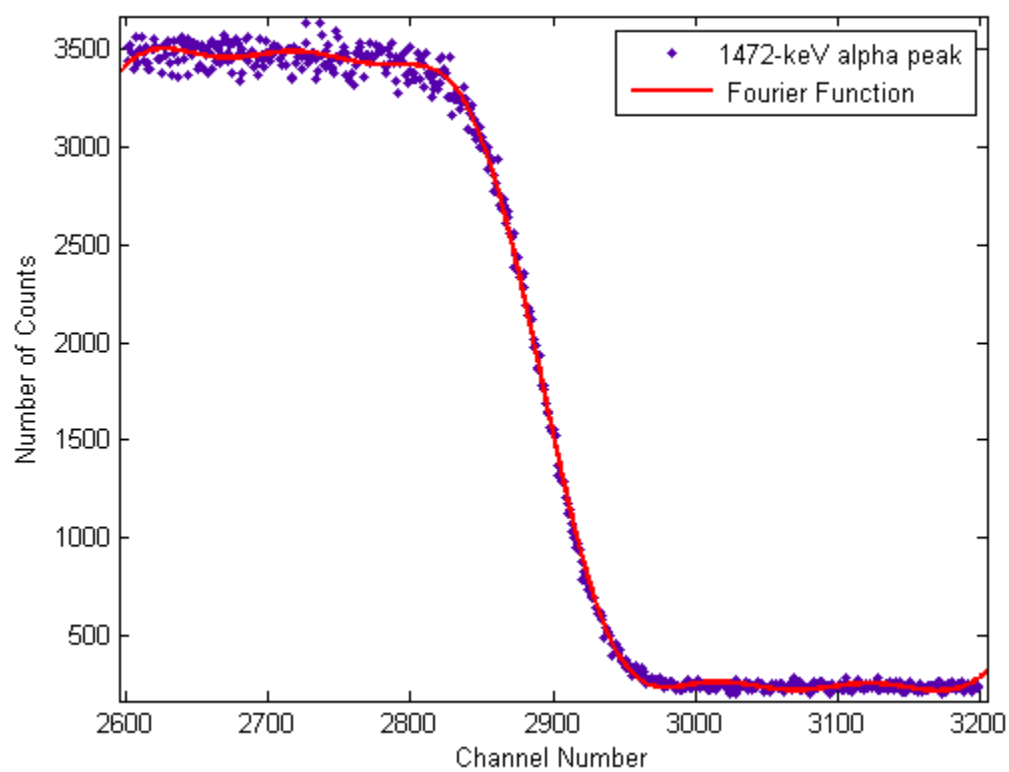
**Figure A-2**: Fourier function fitted to the 1472 keV alpha peak of the measured energy spectrum
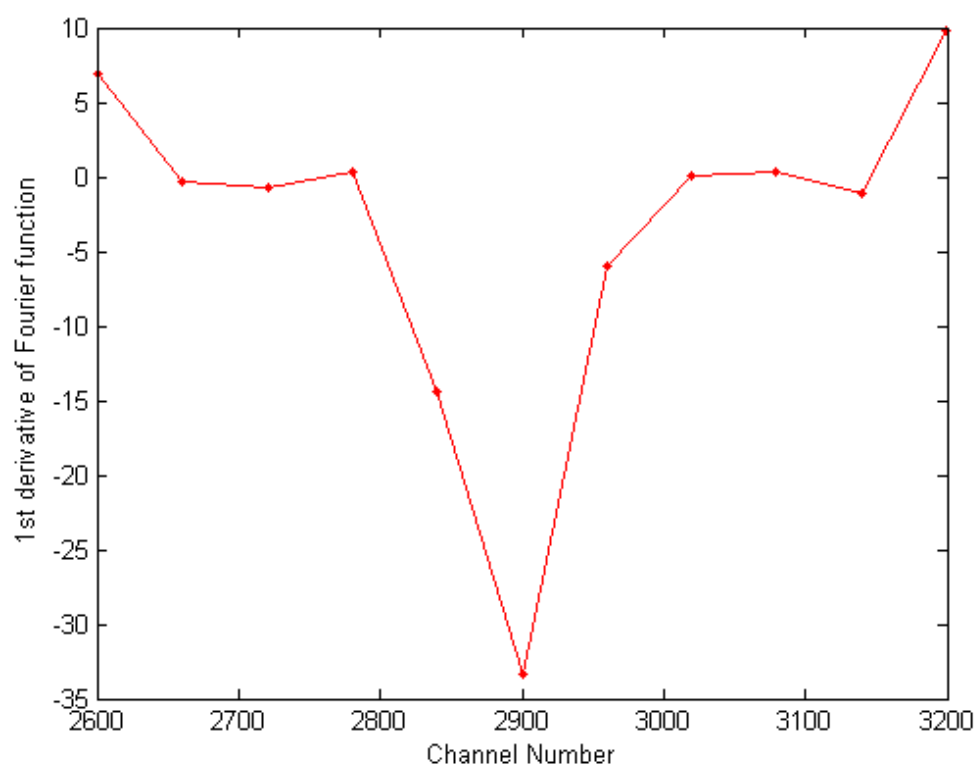
**Figure A-3:** 1st derivative of Fourier function used to locate the center of the peak

**Appendix B**

# Concentration and Depth Calculations

The $^{10}$B concentration profile in the sample is obtained by making deconvolution of the 1472 keV alpha peak in the energy spectrum. This calculation was performed by using the Matlab codes given in Ref. [12]. These codes externally run the SRIM code to calculate the stopping power of the material at different energies. Then, by using the calculated stopping power, concentration profile of $^{10}$B atoms in BPSG sample was obtained by using Equations **2.48** and **2.52** from Chapter **2**.

To calculate the $^{10}$B implantation dose, a NIST standard reference material (SRM-N6) was used. The certified $^{10}$B concentration in N6 is known as $5.22 \pm 0.03 \; x10^{15} \frac{atoms}{cm^2}$. Energy spectrum from SRM-N6 is shown in Figure **B-1**. This spectrum is obtained at the same geometry with BPSG sample. By using the ratio of the areas under the 1472 keV alpha peaks from SRM-N6 and BPSG samples, implanted dose was calculated as $D \cong 6.8 \pm 0.04 \; x10^{16} atoms/cm^2$.

**Table B-1**: The ratio of areas under the 1472 keV alpha peaks from SRN-N6 and BPSG samples

| Sample | Area | Count Time (s) |
|---|---|---|
| SRM-N6 | 90385 | 5.8415E+4 |
| BPSG | 167776 | 8.4005E+3 |

Then, Equation **2-53** was used to calculate the implantation dose value of boron in BPSG sample as,

$$D \left( \frac{atoms}{cm^2} \right) = \frac{167776/84005}{90385/5841.5} * 5.22 \; \pm 0.03 \; x10^{15} \qquad\qquad B.1$$
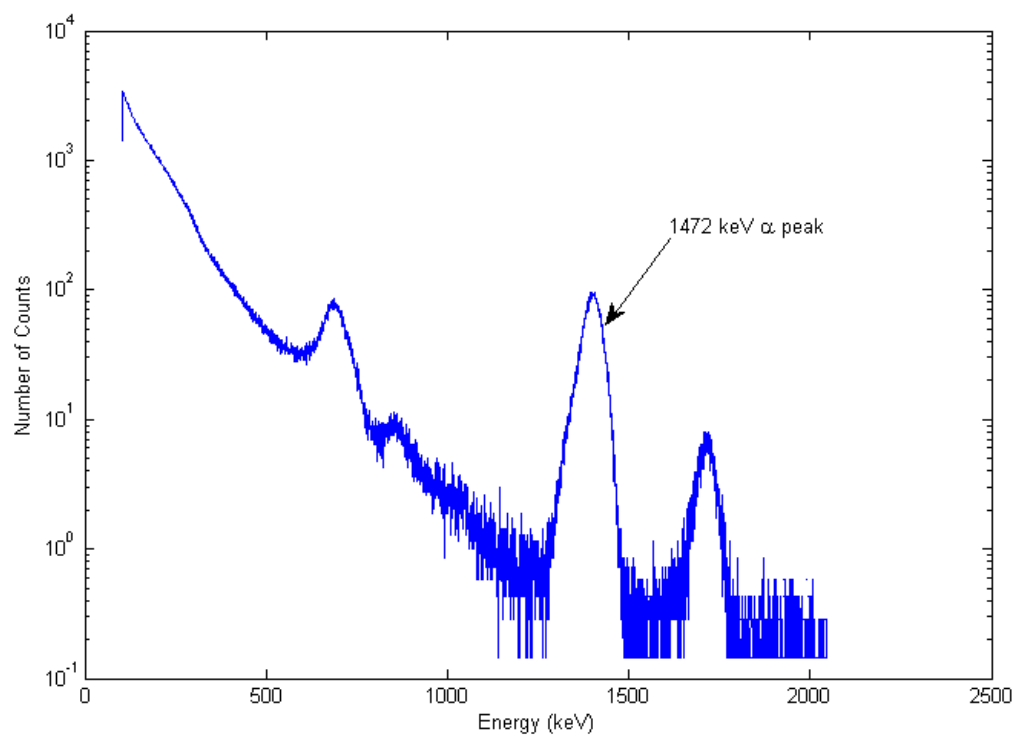
**Figure B-1:** Energy spectrum obtained from SRM-N6 sample by using PIN Photodiode detector at NIST-Cold NDP Facility

**Appendix C**

**GEANT4 Codes**

In this section, some important C++ classes, which were used to model the materials, the neutron beam, tracking of particles, and geometry of the PSU-NDP facility, are given. They were coded in "DetectorConstruction.cc", "PrimaryParticle.cc", and "TrackingSD.cc" classes. The full code package can be obtained by contacting the author of this study.

**i.** **"DetectorConstruction.cc"**

```
#include "DetectorConstruction.hh"

#include "TrackerSD.hh"

#include "G4Material.hh"

#include "G4Box.hh"

#include "G4Tubs.hh"

#include "G4LogicalVolume.hh"

#include "G4ThreeVector.hh"

#include "G4PVPlacement.hh"

#include "globals.hh"

#include "G4MaterialTable.hh"

#include "G4ios.hh"

#include "globals.hh"

#include "G4Element.hh"
```

```cpp
#include "G4PVParameterised.hh"

#include "G4NistManager.hh"

#include "G4SDManager.hh"

#include "G4VisAttributes.hh"

#include "G4AssemblyVolume.hh"


DetectorConstruction::DetectorConstruction() :

        room_log(0), BoroSilicate_log(0),PINPhotodiode_log(0), Silicon_log(0),

        BoroSilicate_phys(0),room_phys(0),PINPhotodiode_phys(0),Silicon_phys(0)

 {;

}

DetectorConstruction::~DetectorConstruction() {

}

G4VPhysicalVolume* DetectorConstruction::Construct() {

//---------Material Construction -------------------------------

G4double a; // atomic mass

G4double z; // atomic number

G4double density;

G4int natoms;

G4int nIsotopes;

G4double weightRatio;

G4String symbol;

G4String name;

G4double abundance;
```

```cpp
G4NistManager* manager = G4NistManager::Instance();

G4Material* Si = manager->FindOrBuildMaterial("G4_Si");

G4Material* Boron = manager->FindOrBuildMaterial("G4_B");

G4Material* Al = new G4Material("Aluminum", z= 13.0, a= 26.98*g/mole, density=

2.7*g/cm3);


G4Isotope* B10 = new G4Isotope(name="B10", 5, 10, a=10.013*g/mole);

G4Isotope* B11 = new G4Isotope(name="B11", 5, 11, a=11.009*g/mole);

G4Element* ele_naturalB = new G4Element("natural B", symbol="naturalB",nIsotopes=2);

ele_naturalB->AddIsotope(B10, abundance=19.9*perCent);

ele_naturalB->AddIsotope(B11, abundance=80.1*perCent);

G4Material* mat_naturalB =new G4Material(name="NaturalB",density=0.1*g/cm3,1);

mat_naturalB->AddElement( ele_naturalB , natoms =1);

G4Material* BSi = new

G4Material(name="BoroSilicate",density=2.23*g/cm3,2,kStateSolid,293.15*kelvin);

BSi->AddMaterial(mat_naturalB, weightRatio=0.042);

BSi->AddMaterial(Si, weightRatio=0.958);

        // The world "material" is vacuum. Parameters used for the definition of "vacuum" are:

        // The material name:

G4String nameVacuum = "Vacuum";

        // The mole mass, density:

G4double densityVacuum = universe_mean_density;

G4double moleMassVacuum = 1.01 * g/mole;

        // The temperature, pressure and atomic number:

G4double pressureVacuum = 3.e-18 * pascal;
```

G4double temperatureVacuum = 293.15 * kelvin;

G4double ZVacuum = 1.;

// Constructing vacuum:

G4Material* vacuum = **new** G4Material(nameVacuum, ZVacuum, moleMassVacuum,

densityVacuum, kStateGas, temperatureVacuum, pressureVacuum);

//---------**Geometry Construction**------------------------------

G4RotationMatrix* yRot = **new** G4RotationMatrix; // Rotates X and Z axes only

yRot->rotateY(-45.0*deg); // Rotates 145 degrees

G4RotationMatrix* yRot2 = **new** G4RotationMatrix; // Rotates X and Z axes only

yRot2->rotateY(135.0*deg);

//Vacuum Chamber

G4double room_x = 3.0*cm;

G4double room_y = 3.0*cm;

G4double room_z = 3.0*cm;

G4Box* room_box = **new** G4Box("room_box",room_x,room_y,room_z);

G4LogicalVolume* room_log = **new** G4LogicalVolume(room_box,vacuum,"room_log");

G4VPhysicalVolume* room_phys = **new** G4PVPlacement(0, // no rotation

G4ThreeVector(0.,0.,0.), // translation position

room_log, // its logical volume

"roomphysics_box", // its name

0, // its mother volume

**false**, // no boolean operations

0); // its copy number

//**Silicon Substrate Material**

G4Box* Silicon = **new** G4Box("Silicate",1.0*cm,1.0*cm,0.5*mm);

G4LogicalVolume* Silicon_log = **new** G4LogicalVolume(Silicon,Si,"Silicon_log");

G4VPhysicalVolume* Silicon_phys = **new** G4PVPlacement(yRot, // no rotation

            G4ThreeVector(0.0*mm,0.0*mm,0.0*mm), // translation position

            Silicon_log, // its logical volume

            "Silicon_sample", // its name

            room_log, // its mother volume

            **false**, // no boolean operations

            0); // its copy number

//**BPSG Sample**

G4Box* BoroSilicate = **new** G4Box("BoroSilicate",1.0*cm,1.0*cm,430*nm);

G4LogicalVolume* BoroSilicate_log = **new**

G4LogicalVolume(BoroSilicate,BSi,"BoroSilicate_log");

G4VPhysicalVolume* BoroSilicate_phys = **new** G4PVPlacement(0, // no rotation

            G4ThreeVector(0.0*mm,0.0*mm,(0.5*mm-600*nm)),

            BoroSilicate_log, // its logical svolume

            "BoroSilicate_sample", // its name

            Silicon_log,    //Silicon_log, // its mother volume

            **false**, // no boolean operations

            0); // its copy number

//**silicon PIN Photodiode Detector**

```
G4Box* PINPhotodiode = new G4Box("PINPhotodiode",5.0*mm,5.0*mm,0.35*mm);

G4LogicalVolume* PINPhotodiode_log = new

G4LogicalVolume(PINPhotodiode,Si,"PINPhotodiode_log");

G4VPhysicalVolume* PINPhotodiode_phys = new G4PVPlacement(yRot2, // no rotation

                G4ThreeVector(1.*cm,0.*m,1.0*cm), // translation position

                PINPhotodiode_log, // its logical volume

                "PINPhotodiode_detector", // its name

                room_log, // its mother volume

                false, // no boolean operations

                0); // its copy number


        // Sensitive Volume

G4SDManager* SDman = G4SDManager::GetSDMpointer();

G4String detectorSDname = "PhotodiodeSD";

TrackerSD* aTrackerSD = new TrackerSD( detectorSDname );

SDman->AddNewDetector( aTrackerSD );

PINPhotodiode_log->SetSensitiveDetector( aTrackerSD );



        //--------- Visualization Attributes -------------------------------


G4VisAttributes* BoxVisAtt= new G4VisAttributes(G4Colour(1.0,1.0,1.0));

G4VisAttributes* BoxVisAtt2= new G4VisAttributes(G4Colour(1.0,1.0,0.0));

G4VisAttributes* BoxVisAtt3= new G4VisAttributes(G4Colour(1.0,0.0,1.0));

G4VisAttributes* BoxVisAtt4= new G4VisAttributes(G4Colour(0.0,0.0,1.0));
```

```
room_log ->SetVisAttributes(BoxVisAtt4);

Silicon_log ->SetVisAttributes(BoxVisAtt2);

BoroSilicate_log ->SetVisAttributes(BoxVisAtt3);

PINPhotodiode_log->SetVisAttributes(BoxVisAtt);

//PIPS_log->SetVisAttributes(BoxVisAtt);

return room_phys;

}
```

## ii.    *"PrimaryGeneratorAction.cc" Class*

```
#include "PrimaryGeneratorAction.hh"

#include "G4Neutron.hh"

#include "G4ParticleTable.hh"

#include "G4NeutronBetaDecayChannel.hh"

#include "G4DecayTable.hh"

#include "globals.hh"

#include "G4RandomDirection.hh"

#include "G4Event.hh"

#include "G4ParticleGun.hh"

#include "G4ParticleTable.hh"

#include "G4ParticleDefinition.hh"

#include<cmath>
```

```
PrimaryGeneratorAction::PrimaryGeneratorAction() {

        G4int n_particle = 1;

        particleGun = new G4ParticleGun(n_particle);

        G4ParticleTable* particleTable = G4ParticleTable::GetParticleTable();

        particleGun->SetParticleDefinition(particleTable->FindParticle("neutron"));

}


PrimaryGeneratorAction::~PrimaryGeneratorAction() {

        delete particleGun;

}


void PrimaryGeneratorAction::GeneratePrimaries(G4Event* anEvent) {

        G4double pos_x;

        G4double pos_y;

        G4double k;

pos_x=(0.5*cm) * G4UniformRand();

pos_y =(0.5*cm) * G4UniformRand();

if(G4UniformRand() < 0.5){

                pos_x=-pos_x;

        }

if(G4UniformRand() < 0.5){

        pos_y=-pos_y;

}

particleGun->SetParticlePosition(G4ThreeVector(pos_x, pos_y, 3.0*cm ));
```

//Maxwell-Boltzmann Energy Distribution modeling by Rejection Technique

```
k = 8.617343e-5 ;

T = 300.;

G4double Eng;

G4double x;

G4double p;

G4double eta1;

G4double eta2;


for (G4int i = 1; i < 10000; i++) {

        eta1 = G4UniformRand();

        eta2 = G4UniformRand();

        x = 0.0029 + eta1 * (0.25 - 0.0029);

        p = 2 * sqrt(x) * exp(-x / (k * T)) / (sqrt(3.1416 * pow((k * T), 3)));

        if (eta2 * 18.7165 <= p) {

                Eng = x*1e-6;

                break;

        }

        }

particleGun->SetParticleEnergy(Eng);

G4ThreeVector v(0.0, 0.0, -1.0);

particleGun->SetParticleMomentumDirection(v);

particleGun->GeneratePrimaryVertex(anEvent);

        }
```

*iii.* **"TrackerSD.cc" Class**

```cpp
#include "TrackerSD.hh"

#include "G4HCofThisEvent.hh"

#include "G4Step.hh"

#include "G4ThreeVector.hh"

#include "G4SDManager.hh"

#include "G4VProcess.hh"

#include "G4Element.hh"

#include "G4ios.hh"

#include <iostream>

#include <fstream>

#include <sstream>

#include <string>

#include <stdio.h>

#include <stdlib.h>

#include "G4UnitsTable.hh"

#include <ctime>


TrackerSD::TrackerSD(G4String name) :

G4VSensitiveDetector(name) {

totalEnergy=0;

stepNumber =0;
```

```
_outPutFile.open("out.txt");

G4String HCname;

collectionName.insert(HCname="trackerCollection");

}

TrackerSD::~TrackerSD() {

_outPutFile.close();

}


void TrackerSD::Initialize(G4HCofThisEvent* HCE) {

trackerCollection = new TrackerHitsCollection(SensitiveDetectorName,collectionName[0]);

static G4int HCID = -1;

if (HCID<0) {

        HCID = G4SDManager::GetSDMpointer()->GetCollectionID(collectionName[0]);

}

        HCE->AddHitsCollection(HCID, trackerCollection);

}

G4bool TrackerSD::ProcessHits(G4Step* _aStep, G4TouchableHistory*) {

aStep=_aStep;

stepNumber += 1;

if (aStep->GetTotalEnergyDeposit()==0.)

        return false;

        edep += aStep->GetTotalEnergyDeposit();

        return true;

}
```

```
void TrackerSD::EndOfEvent(G4HCofThisEvent*) {

if (edep<=0.0){

        return;

}


if (!_outPutFile) {

        _outPutFile << "Could not create the output file. \n";

        return;

}

        _outPutFile <<edep*1e+3<< G4endl;

        edep=0;

        }
```

## Appendix D

## Energy Spectrum Plotting

To plot the energy spectrum of the emitted particles from the neutron induced reactions in Geant4 simulation, a Matlab script was written. It was named as *"spectra.m"*, and is given below. The result of Geant4 simulation is a file which contains the kinetic energy of each detected particle/or atom by the photodiode detector in the unit of keV. The name of the file is *"out.txt"*. This file is opened by the code by using *fopen* command, and then each calculated energy value is loaded into an array by using *textread* command. Energy and channel numbers are calculated by using the algorithm given in Equation **5.2** in Section **5.3**.

**"Spectra.m"**

```
fid2=fopen('out.txt');

[a,b,c]=textread('out.txt', '%f%f %f ');

        for k = 1:N        %N is the number of energy values stored in the 'out.txt'

                E(k,1) = a(k);

        end

fclose(fid2);

        for i=1:4096

                count(i,1)=0;

        end

k=0;

        for j=1:4096
```

```
for i=1:280058

    if( E(i,1)> (j-1)*0.5079  &&  E(i,1)<j*0.5079 )

        count(j,1)=count(j,1)+1;

    end

    energy(j,1)=( (j-1)*0.5079 + j*0.5079 )/2;

end

end

plot(energy(:,1),count(:,1));
```